Long-Term Tectono-Stratigraphic Evolution of a Propagating Rift System, L'Aquila Intermontane Basin (Central Apennines)

Giorgio Arriga, Marta Marchegiano, Marion Peral, Hsun-ming Hu, Domenico Cosentino, Chuan-chou Shen, Hayden Dalton, Mauro Brilli, Luca Aldega, Philippe Claeys, et al.

Tectonics®

RESEARCH ARTICLE
10.1029/2024TC008548

Key Points:

- En-echelon seismogenic faults in L'Aquila Basin exhibit polyphase tectonic activity with stages of nucleation, localization and interaction
- Transition from soft- to hard-linkage controlled basin evolution and Middle-Upper Pleistocene sedimentation
- Tectonic interplay among the various seismogenic faults regulate the seismotectonic setting of the region

Supporting Information:

Supporting Information may be found in the online version of this article.

Correspondence to:

G. Arriga,
giorgioarriga@uniroma3.it

Citation:

Arriga, G., Marchegiano, M., Peral, M., Hu, H.-M., Cosentino, D., Shen, C.-C., et al. (2024). Long-term tectono-stratigraphic evolution of a propagating rift system, L'Aquila Intermontane Basin (central Apennines). *Tectonics*, *43*, e2024TC008548. https://doi.org/10.1029/2024TC008548

Received 8 AUG 2024
Accepted 12 NOV 2024

Author Contributions:

Conceptualization: Giorgio Arriga, Domenico Cosentino, Federico Rossetti
Data curation: Giorgio Arriga, Federico Rossetti
Formal analysis: Giorgio Arriga, Marta Marchegiano, Marion Peral, Hsun-Ming Hu, Chuan-Chou Shen, Hayden Dalton, Mauro Brilli, Luca Aldega
Funding acquisition: Domenico Cosentino, Philippe Claeys, Federico Rossetti
Investigation: Giorgio Arriga, Marta Marchegiano, Marion Peral, Hsun-Ming Hu, Domenico Cosentino, Chuan-Chou Shen, Hayden Dalton, Mauro Brilli, Luca Aldega, Federico Rossetti
Methodology: Marta Marchegiano
Supervision: Marta Marchegiano, Marion Peral, Domenico Cosentino, Philippe Claeys, Federico Rossetti
Validation: Marta Marchegiano, Marion Peral, Hsun-Ming Hu, Domenico Cosentino, Chuan-Chou Shen,

Long-Term Tectono-Stratigraphic Evolution of a Propagating Rift System, L'Aquila Intermontane Basin (Central Apennines)

Giorgio Arriga[1,2], Marta Marchegiano[2,3], Marion Peral[2,4], Hsun-Ming Hu[5,6], Domenico Cosentino[1], Chuan-Chou Shen[5,6], Hayden Dalton[7], Mauro Brilli[8], Luca Aldega[9], Philippe Claeys[2], and Federico Rossetti[1]

[1]Department of Science, University of Roma TRE, Rome, Italy, [2]Archaeology, Environmental Changes, and Geo-Chemistry, Vrije Universiteit Brussel (VUB), Brussels, Belgium, [3]Department of Stratigraphy and Paleontology, University of Granada, Granada, Spain, [4]EPOC, UMR 5805 University of Bordeaux CNRS, Pessac, France, [5]High-Precision Mass Spectrometry and Environment Change Laboratory (HISPEC), Department of Geosciences, National Taiwan University, Taipei, Taiwan (Republic of China), [6]Research Center for Future Earth, National Taiwan University, Taipei, Taiwan (Republic of China), [7]School of Geography, Earth and Atmospheric Sciences, The University of Melbourne, Parkville, VIC, Australia, [8]Istituto di Geologia Ambientale e Geoingegneria (IGAG), Consiglio Nazionale delle Ricerche (CNR), Rome, Italy, [9]Dipartimento di Scienze della Terra, Sapienza Università di Roma, Rome, Italy

Abstract Understanding the long-term tectono-stratigraphic evolution of active extensional faulting is crucial for unraveling the mode through which continental rifting propagates in space and time. The Pliocene-Quaternary L'Aquila Intermontane Basin (AIB) in central Apennines offers a natural laboratory for studying a propagating continental rift. Seismicity is related to NW-SE-striking normal faults that have been accommodating crustal stretching since the Late Pliocene. Through a multidisciplinary approach integrating field, mineralogical, geochemical (C-O stable and clumped isotopes) and geochronological ($^{40}Ar/^{39}Ar$, U-Th) analyses, this study focuses on the structural connection between the Mount Pettino Fault (MPF) and the Paganica Fault, two active, left-stepped basin boundary faults of the AIB. A two-stage tectono-stratigraphic evolution is proposed during transition from localized to delocalized deformation and fault linkage. Stage-1 (pre-Middle Pleistocene) corresponds to nucleation and growth of the MPF, characterized by a ∼5 m thick exhumed fault core, consisting of an isotopically closed cataclasite (T (Δ_{47}) ∼33–50°C). Stage-2 corresponds to the development of a distributed zone of NW-SE and E-W extensional faulting in the overlay zone with the Paganica Fault, which is interpreted as a transfer zone linking the basin boundary faults, with maximum long-term slip rates comparable to those of the connected faults. Structurally controlled circulation of meteoric fluids promoted carbonate veining and travertine formation (T (Δ_{47}) ∼8°C). U-Th carbonate dating of Stage-2 mineralizations constrains the tectonic activity in the transfer zone at least at ∼182–331 ka. Implications on the tectono-stratigraphic evolution and on the seismotectonic scenario of the AIB are discussed, providing geodynamic inference at regional scale.

Plain Language Summary We studied how crustal stretching has been accommodated in the Apennine Mountains of central Italy during the Middle-Late Pleistocene. By studying the L'Aquila Intermontane Basin, a Late Pliocene-Quaternary sedimentary basin bounded by extensional faults, we investigated how the basin boundary faults evolve and connect over time. Using a variety of methods including fieldwork, mineralogical, geochemical and geochronological analyses, we focused on the overlapping zone between the Mount Pettino and the Paganica active extensional faults. We found that the Mount Pettino Fault experienced a two stage evolution, with the first stage involving the growth of the fault zone at depth, followed by exhumation and connection with the Paganica Fault. Fault linkage was associated with formation of diffuse carbonate veining and travertine deposition during the ∼182–331 ka time lapse. Such tectonic interaction contributed to reshape the basin architecture, transforming it from two separated, internally drained sub-basins into a single, interconnected basin with external drainage. Results contribute to refine our understanding of how active extensional faulting nucleated, developed and interacted in space and time in the central Apennines.

Hayden Dalton, Luca Aldega, Philippe Claeys, Federico Rossetti
Visualization: Giorgio Arriga
Writing – original draft: Giorgio Arriga, Domenico Cosentino, Philippe Claeys, Federico Rossetti
Writing – review & editing: Giorgio Arriga, Marta Marchegiano, Marion Peral, Domenico Cosentino, Luca Aldega, Philippe Claeys, Federico Rossetti

1. Introduction

The tectonic and structural evolution of continental rifting depends on numerous (far- to near-field) factors, spanning from the geodynamic scenario to rheology of the lithosphere, stretching rate and direction (Bassi, 1991; Buck, 1991; Mondy et al., 2017; Olsen, 1995; Reston & Pérez-Gussinyé, 2007; Rosenbaum et al., 2008; Sawyer et al., 2007; Van Wijk & Blackman, 2005). The mode through which extensional tectonics is accommodated in the continental crust involves fault growth, linkage, and coalescence (Cartwright et al., 1995; Cowie & Scholz, 1992; Crone & Haller, 1991; Fossen & Rotevatn, 2016; Peacock & Sanderson, 1991; Peacock et al., 2000; Trudgill & Cartwright, 1994; Walsh & Watterson, 1991; Walsh et al., 2003). To understand rift systems development and propagation, it is therefore essential to investigate the interaction of the different fault strands and their connection through space and time to form the basin boundary faults (Duffy et al., 2015; Ebinger, 2005; Trudgill & Cartwright, 1994; Zwaan et al., 2016).

Because the space-time evolution of extensional fault systems is responsible for the differential subsidence in the extending crust, their structural connection strongly affects local depocenters and facies distribution at the fault hanging walls (Gawthorpe & Hurst, 1993; Gupta et al., 1998; Larsen, 1988). Therefore, sedimentation within extensional basins evolves as rift systems become more mature and connected at the surface (e.g., Gawthorpe & Leeder, 2000). Hence, understanding the evolution of extensional basins is critical in assessing the long-term tectonic evolution of continental rifting, with insights into the seismotectonic framework of the basin boundary faults (e.g., Crone & Haller, 1991; Galli et al., 2011).

The central sector of the Apennines is one of the most seismically active regions of the Mediterranean area (Giardini et al., 2003). Seismicity is controlled by the activity of a set of NW-SE-striking high-angle normal fault systems (Figure 1a) that has been accommodating the post-orogenic extensional stretching of the Apennine belt since the Late Pliocene (∼3 Ma) with formation of distributed intermontane basins (Cosentino et al., 2010 and references therein; Figure 1b).

Within this seismotectonic setting, the fault-controlled sedimentary basins along the Aterno River system provide a natural laboratory to study the space-time fault interaction and their control on subsidence and sedimentation in active extensional settings (Cosentino et al., 2017; Geurts et al., 2018) (Figure 1). Presently, the drainage of the Aterno River system connects several NW-SE oriented extensional basins, encompassing, from north to south, the Montereale (MTR), L'Aquila (AIB), Lower Aterno-Subequana (LAS), and Sulmona (SUL) intermontane basins (Geurts et al., 2020; Figure 1b). The tectono-stratigraphic evolution of these basins is controlled by the space-time evolution of the Aterno Fault System, which comprises several NW-SE-striking fault strands, with a cumulative length of 50–60 km and en-echelon geometry (Boncio et al., 2004; Galli et al., 2008; Iezzi et al., 2019; Roberts & Michetti, 2004) (Figure 1). Despite the seismogenic fault pattern is characterized by discrete fault segmentation at the surface, suggesting that faults are separated structures (e.g., Gori et al., 2012), seismological data indicate a structural connection (e.g., Falcucci et al., 2015; Figure 1c). This scenario is well documented by the Mw 6.3, 6 April 2009, L'Aquila earthquake. Indeed, while the surface ruptures were distributed within a 13 km-wide area along the NW-SE striking eastern boundary faults of the AIB (the so-called Paganica-San Demetrio fault system in Boncio et al. (2010)), the associated seismic sequence propagated within a 20–30 km long NW-SE oriented rift system (Figure 1c) (Cheloni et al., 2010; Chiaraluce et al., 2011; D'Agostino et al., 2012; Di Luccio et al., 2010; Di Stefano et al., 2011; Lavecchia et al., 2012). This evidence indicates the tectonic interplay of the seismogenic structures at depth, not matched by the fault ruptures at the surface.

Moreover, paleoseismological investigations highlighted that the entire fault system can activate simultaneously, generating larger magnitude earthquakes in the past (e.g., the 1703 Mw 6.7 seismic sequence, Galli et al., 2011; Figure 1d). A structural connection among the basin boundary faults of the AIB is also consistent with the continuity of the stratigraphical record along the basin. However, although the seismotectonic scenario of the AIB has been assessed previously, the long-term tectono-stratigraphic response of the brittle extending crust is still poorly defined, hampering the understanding of how the major fault systems nucleated, propagated, and interacted during rift propagation in the region.

To achieve this goal, we investigate the tectono-stratigraphic architecture of the overlay zone between the Mount Pettino Fault (MPF) and the Paganica Fault (PGF), two seismogenically active left-stepped fault segments, forming the NE basin boundary faults of the AIB (Figure 1a). By focusing on the MPF, a punctuated history of fault slip and sedimentation/erosion is documented, which involved transition from fault localization,

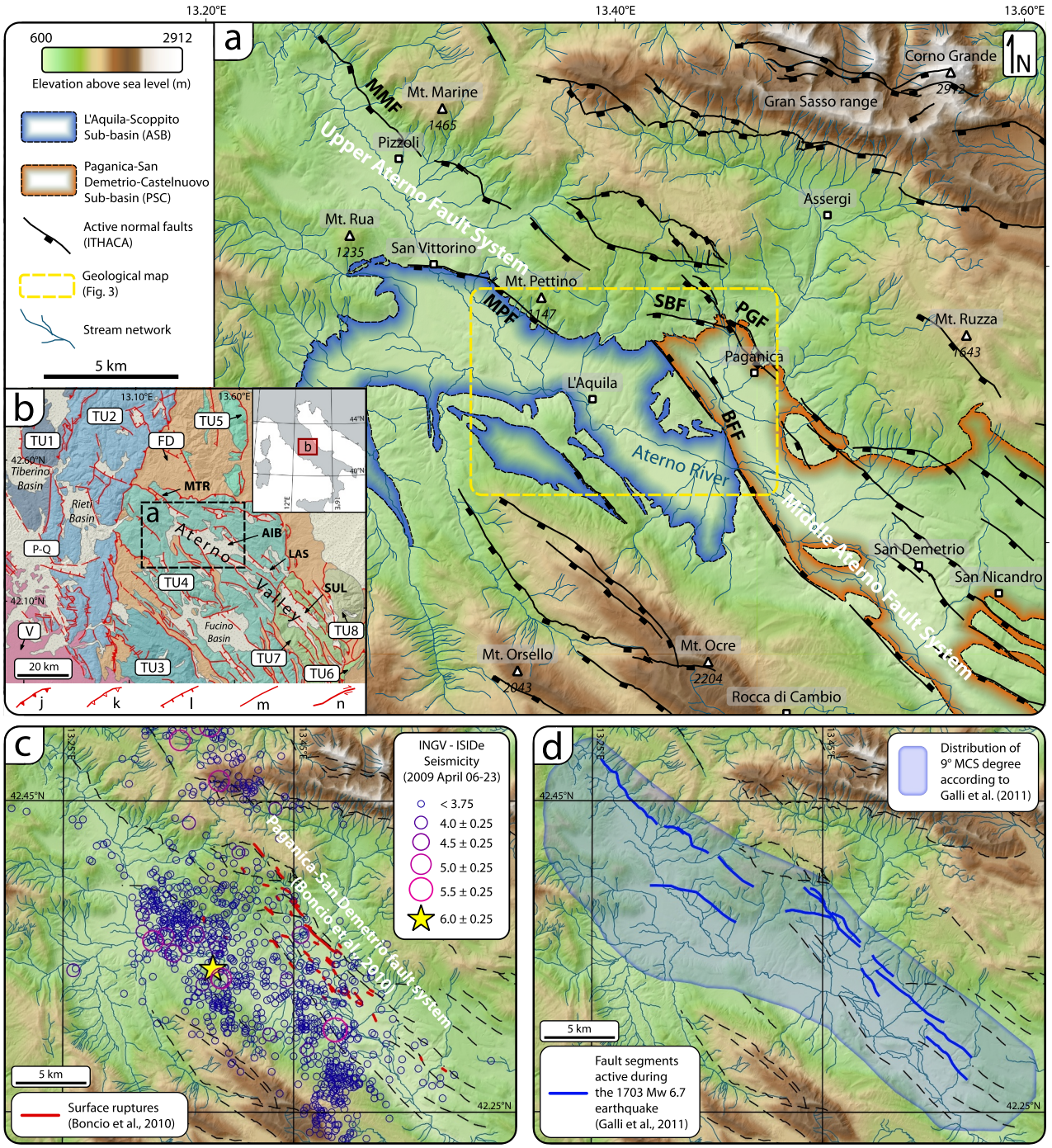

Figure 1. (a) Topographic map with seismogenic fault pattern of the Upper and Middle Aterno Fault systems showing active normal faults from the database of ITaly HAzards from CApable faulting (ITHACA, 2019) and the sediment distribution of the L'Aquila-Scoppito (ASB) and Paganica-San Demetrio-Castelnuovo (PSC) sub-basins. MMF: Mount Marine Fault; MPF: Mount Pettino Fault; SBF: San Biagio Fault; PGF: Paganica Fault. (b) Structural map of the main tectonic units (TU) of central Apennines and Intermontane Basins (modified after Cosentino et al. (2017)). TU1: Inner Umbria Tectonic Unit; TU2: Umbria-Marche-Sabine Tectonic Unit; TU3: Simbruini-Ernici-Matese Tectonic Unit; TU4: Gran Sasso-Western Marsica Tectonic Unit; TU5: Acquasanta-Montagnone Tectonic Unit; TU6: Molise Tectonic Unit; TU7: Morrone-eastern Marsica Tectonic Unit; TU8: Maiella Tectonic Unit; FD: undistinguished Foredeep deposits; V: Quaternary volcanic rocks; P-Q: Plio-Quaternary continental deposits; (j) major thrust; (k) minor thrust; (l) normal fault; (m) undifferentiated fault; (n) strike-slip fault. The map shows the location of the Aterno Valley, which traverses several fault-bounded intermontane basins, including the Montereale (MTR), L'Aquila (AIB), Lower Aterno-Subequana (LAS), and Sulmona (SUL) basins. (c) Distribution of the seismicity related to the Mw 6.3, 2009, April 6 L'Aquila earthquake 17 days after the main shock (ISIDe, 2007) and associated surface ruptures (Boncio et al., 2010). (d) Fault pattern activated during the 1703 Mw 6.7 earthquake (Galli et al., 2011). The area in blue represents the distribution of the 9° of the MCS intensity scale associated with the event.

segmentation to linkage that is constrained in the last 400 kyr. When these new tectono-stratigraphic data are integrated with the regional scenario, the anatomy of the rift system leading to formation of the AIB can be reconstructed, providing new insights into the seismotectonic scenario accompanying the Late Pliocene-Quaternary rifting in central Apennines.

2. Geological Background

The Apennine chain is a Cenozoic orogenic belt formed by the westward subduction of the Adriatic microplate below the Eurasian plate (Carminati & Doglioni, 2012; Cosentino et al., 2010; Faccenna, Becker, Auer, et al., 2014; Royden et al., 1987). The chain arches along the Italian Peninsula and is subdivided into three main (northern, central, and southern) sectors having different kinematic evolution, tectonic styles, stratigraphy, and structural architecture (Butler et al., 2004; Carannante et al., 2013; Cipollari & Cosentino, 1996; Cosentino et al., 2010; Elter et al., 2012; Lanari et al., 2023; Patacca et al., 1990).

The central sector (central Apennines) is structured into a NE-verging fold-and-thrust belt made of Mesozoic-Cenozoic carbonate successions and Miocene-Pliocene siliciclastic foredeep deposits (Cosentino et al., 2010). Orogenic deformation is constrained by the age of the foredeep and thrust-top basins, K-Ar ages of fault gouge and U-Pb dating of calcite slickenfibers from the main thrusts, which shows a migration of the compressional fronts from the Tyrrhenian to the Adriatic side starting from the late Burdigalian (~18 Ma) to the Late Pliocene (~3 Ma) (Bally, 1986; Carboni et al., 2020; Centamore & Rossi, 2009; Cipollari & Cosentino, 1995, 1996; Cipollari, Cosentino, Esu, et al., 1999; Cipollari, Cosentino, & Gliozzi, 1999; Cosentino et al., 2010; Curzi et al., 2020; Curzi, Cipriani, et al., 2024; Elter et al., 2003; Endignoux et al., 1989; Patacca & Scandone, 1989; Patacca et al., 1990, 2008; Sage et al., 1991; Tavani et al., 2023).

The central Apennine chain initially developed with a piggy-back structural style (Cosentino et al., 2010), which subsequently experienced at least two out-of-sequence compressional phases that reactivated pre-existing deformation fronts with N-S and E-W structural directions. These events are represented by the Olevano-Antrodoco-Monte Vettore thrust system (Late Messinian, ~5–6 Ma) and the Gran Sasso thrust front (Late Zanclean, ~3–4 Ma), respectively (Cavinato et al., 1986; Cosentino et al., 2010; Ghisetti & Vezzani, 1991; Salvini & Vittori, 1982).

The present-day tectonic setting of the central Apennines is controlled by post-orogenic extensional tectonics, active since the Late Pliocene–Early Pleistocene (Bosi & Messina, 1991; Patacca et al., 1990). Extensional tectonics reworked the earlier nappe stack through normal faults striking sub-parallel to the chain axis (Bigi et al., 1992; Parotto & Praturlon, 1975). Extensional faulting is also responsible for the active seismicity in the region, distributed along the divide of the Apennine chain. These faults are responsible for several recent and historical earthquakes with Mw up to 6–7 (Blumetti & Guerrieri, 2007; Galadini & Galli, 2000; Galli et al., 2010, 2011; Storti et al., 2013; Vittori et al., 2011).

The extensional tectonics in the central Apennines is described as a two-stage process. The first stage is related to the Tyrrhenian back-arc extension induced by the progressive retreat of the Adria subducting plate, active since the Middle Miocene with a general eastward migration from the hinterland of the chain (Carminati & Doglioni, 2012; Cavinato & Celles, 1999; Cipollari, Cosentino, & Gliozzi, 1999; Cosentino et al., 2010; Faccenna et al., 1997, 2001; Galadini & Messina, 2004; Patacca et al., 1990). The second stage corresponds to the collapse of the orogen (Dewey, 1988), active since the Late Pliocene. Slab break-off and opening of the Adriatic slab window are thought to be the main geodynamic engines of extensional faulting and regional uplift (Cosentino et al., 2017; D'Agostino et al., 2001; Faccenna, Becker, Auer, et al., 2014; Fellin et al., 2021; Lanari et al., 2023; San Jose et al., 2020; Racano et al., 2024). The uplift in the central portion of the belt, with rates up to 1–2 mm/yr (Serpelloni et al., 2013), is thought to be assisted by the convecting mantle (Faccenna, Becker, Miller, et al., 2014; Racano et al., 2024; San Jose et al., 2020). Extensional faulting was responsible for the opening of several Late Pliocene-Quaternary extensional intermontane basins (Cosentino et al., 2010; Galadini, 1999; Galadini et al., 2003, 2012; Lanari et al., 2021), filled by alluvial, fluvial, and lacustrine deposits (Cavinato & Celles, 1999; Cavinato et al., 1994; Cosentino et al., 2017). These extensional basins experienced multiple transitions from endorheic to exorheic drainage over time, due to interplay among climate, fluvial incision, sediment supply, and tectonics (Geurts et al., 2018, 2020).

It is still challenging to discriminate and quantify the relative impact of the two-stage extensional tectonics in shaping and controlling the evolution of the post-orogenic subsidence and sedimentation in the intermontane basins of the central Apennines. In fact, while it is commonly assumed that the onset of the intermontane extension shifts spatially and temporally following the thrust emplacement (e.g., Cavinato & Celles, 1999), the recent studies of Cosentino et al. (2017), Spadi et al. (2018, 2019), and Mondati et al. (2021) suggest a synchronous formation of some of the main central Apennine intermontane basins.

2.1. Tectono-Stratigraphic Setting of the AIB

The AIB is one of the main post-orogenic extensional basins of the central Apennines (Figure 1b). Located in the central portion of the Aterno Valley, it is bounded by the Gran Sasso Range to the north, and the D'Ocre Mountains to the south. Subsidence has occurred since the Late Piacenzian-Early Gelasian hosting a succession of continental deposits structurally controlled by the activity of high-angle normal faults (Cosentino et al., 2017; Tallini et al., 2019).

The geology and the stratigraphic succession of the AIB have been investigated with surface surveys (Bertini & Bosi, 1993; Giaccio et al., 2012; Nocentini et al., 2017, 2018; Pucci et al., 2019) and subsurface data, as derived from interpretation of seismic reflection lines (Cosentino et al., 2017; Improta et al., 2012; Tallini et al., 2012, 2019), boreholes (Amoroso et al., 2010; GEMINA, 1963), and airborne LiDAR (Civico et al., 2017).

The depositional system is characterized by a succession of multiple sedimentary bodies bounded by erosional surfaces (synthems) and characterized by variable lateral thicknesses. These synthems unconformably overlie the deformed pre- and syn-orogenic successions, composed of Jurassic-Middle Miocene carbonate and Upper Miocene siliciclastic rocks, respectively (Centamore & Dramis, 2010; Vezzani & Ghisetti, 1998).

The AIB is subdivided into two main sub-basins, which experienced different evolutions in terms of tectonic activity and depositional history (Cosentino et al., 2017; Giaccio et al., 2012; Nocentini et al., 2017, 2018). The eastern portion consists of the Paganica-San Demetrio-Castelnuovo Sub-basin (PSC; Figure 1a). The PSC extends with a NW-SE direction, from Paganica to San Nicandro and encompasses several active faults strands related to the Middle Aterno Fault System (Figure 1a). The PSC is a graben structure, bordered by two main NW-SE-oriented normal faults: the Paganica Fault (PGF) to the east, and its antithetic Bazzano-Fossa Fault (BFF) to the west, respectively (Figure 1a).

The western portion of the AIB corresponds to the L'Aquila-Scoppito Sub-basin (ASB, Figure 1a), developed within the southern margin of the Upper Aterno Fault System (Figure 1a). The ASB is bordered to the north by the MPF, representing the main boundary fault of the basin, which thus exhibits a half-graben geometry.

To the north, the junction between the ASB and the PSC is constituted by the overstep zone between the MPF and the PGF, which comprises the active San Biagio Fault (SBF) (ITHACA, 2019; Figure 1a), also called the Colle Frolla Fault (COF) (Guerrieri et al., 2010; Vittori et al., 2011). The zone encompassing the San Biagio and the Paganica faults, represents the junction between the Upper and the Middle Aterno Fault systems (Figure 1a), which includes several seismogenic fault segments (Boncio et al., 2004; Galli et al., 2008; Iezzi et al., 2019; Roberts & Michetti, 2004; Villani et al., 2016). The two sub-basins are separated by the BFF.

According to Nocentini et al. (2017, 2018), the sedimentary infilling of the AIB can be subdivided into three main stratigraphic units, from bottom to top (Figure 2): (a) Unit-1 (Upper Pliocene-Lower Pleistocene p.p.), forming the basal stratigraphic deposits of the AIB. In the western portion (ASB), it is entirely composed of the Colle Cantaro-Cave synthem (Centamore & Dramis, 2010), which, consisting of slope-derived breccias and debris flow deposits Nocentini et al. (2017), has been attributed to the syn-rift stage of the basin (Cosentino et al., 2017). In the eastern portion (PSC), the syn-rift Unit-1 is less developed and is covered by a thick succession of lacustrine deposits related to the San Demetrio-Colle Cantaro Cave synthem, which is absent in the ASB (Figure 2). (b) Unit-2 (Lower Pleistocene p.p.), consisting of a 200 m-thick fluvio-lacustrine succession (Amoroso et al., 2010; Cosentino et al., 2017; Tallini et al., 2012) of stratified yellowish/gray clayey and silt layers with coarse sand and conglomerate beds, including five horizons of lignite (Cosentino et al., 2017; GEMINA, 1963) and large mammals remains (Agostini et al., 2012; Maccagno, 1962, 1965; Magri et al., 2010; Mancini et al., 2012). This fluvio-lacustrine succession corresponds to the Madonna della Strada synthem (MDS) (Centamore & Dramis, 2010; Cosentino et al., 2017; Nocentini et al., 2017) and is exposed almost entirely in the ASB. Tallini et al. (2019), by considering the 400 m of fine-grained siliciclastic deposits drilled by the S10 borehole, show a

10.1029/2024TC008548

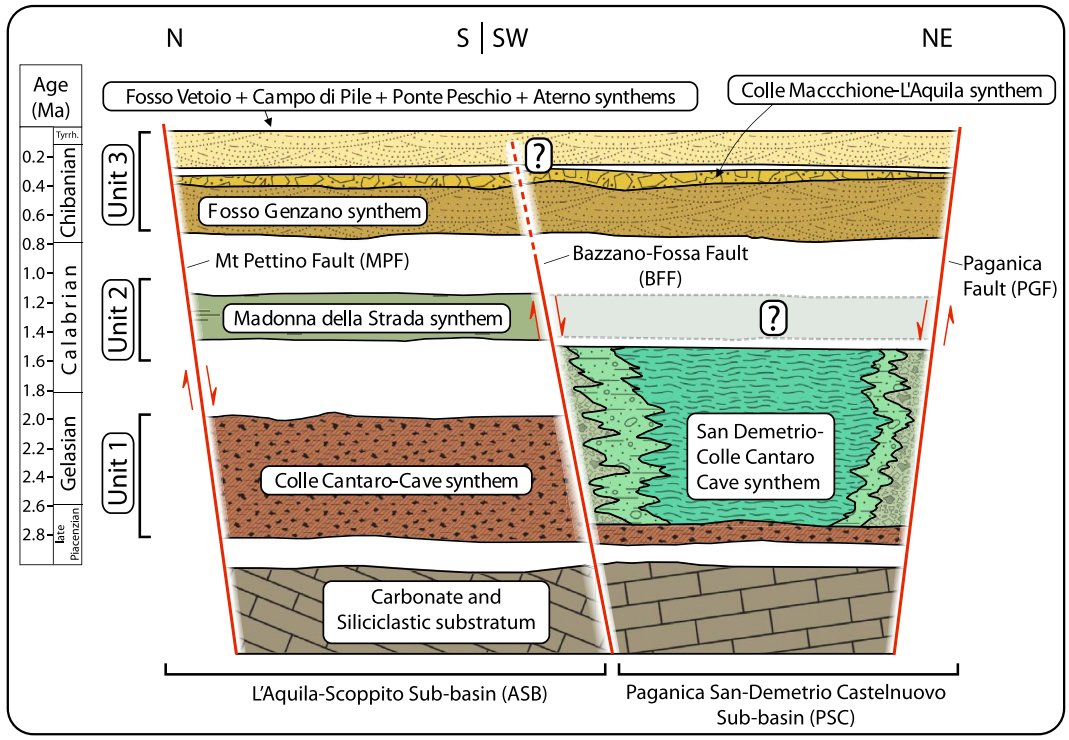

Figure 2. Simplified tectono-stratigraphic scheme of the Plio-Quaternary stratigraphic succession of the L'Aquila-Scoppito and Paganica-San Demetrio-Castelnuovo sub-basins and their master faults (modified respectively after Cosentino et al. (2017) and Nocentini et al. (2018)). The sedimentary succession is characterized by continental fluvial-alluvial-lacustrine deposits organized in synthems, bounded by erosional unconformities. In this work we subdivided the synthems in three main units based on lithological characteristics and their relation to tectonics, representing three different stages of the evolution of the AIB. Unit 1 corresponding to the first depositional cycle, started in the late Piacenzian-early Gelasian. In the L'Aquila-Scoppito Sub-basin, it is entirely composed of the syn-rift deposits of the Colle Cantaro-Cave synthem, whilst in the Paganica-San Demetrio-Castelnuovo Sub-basin it is also characterized by the presence of fluvial/lacustrine deposits (absent in the other sub-basin). Unit 2, mainly included in the Calabrian stage, is characterized by the Madonna della Strada Fm. and is prevalent in the ASB, while in the PSC it is very rare or absent (Figure 3). Unit 3 includes the Middle to Upper Pleistocene fluvial and alluvial deposits of the Aterno River, distributed equally between ASB and PSC.

possible MDS depocenter beneath L'Aquila downtown. (c) Unit-3 (Middle Pleistocene-Holocene) continuously cropping out in both sub-basins, consists of a succession of fluvial and alluvial stratigraphic units, marked by erosional surfaces (synthems), related to the dynamics of the Aterno River and its tributaries, stratigraphically constrained from 0.78 Ma to Present (Cosentino et al., 2017). The fluvial and alluvial succession linked to the Aterno River dynamics is interspersed by a late Middle Pleistocene episode of rock avalanche known as the Colle Macchione-L'Aquila synthem (L'Aquila Breccias Fm.) (Antonielli et al., 2020; Cosentino et al., 2017). The stratigraphic transition from lacustrine-to fluvial-dominated sedimentation has been interpreted to record an evolution from an endorheic to exorheic phase at about 1.1–1.2 Ma, with the first surface fluvial connection at 0.8–0.6 Ma, as documented by the oldest alluvial deposits related to Fosso Genzano synthem (Geurts et al., 2020; Nocentini et al., 2017).

2.2. The Mount Pettino Fault (MPF)

The MPF is part of the SW-dipping, en-echelon seismogenic fault network that, together with the Mount Marine Fault to the NW, and the PGF to the SE, defines the northeastern basin boundary fault system of the AIB (Figure 1a).

The MPF strikes NW-SE and dips SW with an angle of 65–70° defining a 0.5–1-km long badland zone exposed along the piedmont of the Mount Pettino Ridge, from San Vittorino (NW) to L'Aquila town (SE) (Figure 1a). In its central sector, the MPF juxtaposes the shallow-water limestones of the Calcare Massiccio Fm. (Hettangian-lower Pliensbachian) on the footwall, with the deep-water limestones of the Maiolica Fm. (lower Tithonian-lower

Aptian) on the hanging wall. Based on the stratigraphic separation between these formations, as reported in the 359-L'Aquila geological map (Centamore et al., 2006), the displacement of the MPF is about 1.5–2 km (Iezzi et al., 2019).

The total length of the MPF has been reconstructed by seismic reflection profiles that indicate a length of ∼7–8 km (Nocentini et al., 2017; Tallini et al., 2019). The paleoseismological investigations along the MPF have documented Holocene colluvial wedge deposits (dated up to 8600–8440 years BP; Galli et al., 2011) displaced by high-angle extensional faults, with an average slip rate of ∼0.6 mm/yr (Galli et al., 2011). By analyzing the active fault scarps along the MPF from LiDAR data, Brunori et al. (2013) estimated a slip rate of 0.6–1.1 mm/yr, whereas Galadini and Galli (2000), inferred a vertical slip rate of 0.47–0.86 mm/yr for the last 31,710 ± 760 years through the analysis of displaced terraced surfaces.

Toward SE, the cataclastic badland zone, corresponding to the main trace of the MPF, is buried below a 50–100 m-thick clastic deposits forming the near-surface substrate of the L'Aquila Town. These deposits consist of the Middle Pleistocene L'Aquila Breccias Fm. (∼350 ka; Nocentini et al., 2017) and the overlying Collemaggio synthem (MIS 5e, ∼125 ka; Nocentini et al., 2017; Tallini et al., 2019). Through the interpretation of a seismic line crossing L'Aquila Town, Tallini et al. (2019) defined the southeastward prosecution of the MPF. In this sector, minor normal faults cut across the L'Aquila Breccias Fm., with a cumulative fault displacement in the order of ∼15 m (see section C-C′ in Nocentini et al. (2017)). It is worth to note that these faults are sealed by the Collemaggio synthem (Nocentini et al., 2017; Tallini et al., 2019). Considering the time lag between the age of the L'Aquila Breccias Fm. and the age of the Collemaggio Fm., the long-term (350–125 kyr) slip rate along this portion of the MPF is around 0.07 mm/yr.

The structural and seismic interplay among the different seismogenic fault segments is still unclear, as they exhibit different behavior during distinct seismic sequences. The distribution of the surface ruptures following the 2009 Mw 6.3 L'Aquila earthquake indicates a propagation of the deformation in correspondence of the Paganica Fault, bypassing the MPF (Boncio et al., 2010). Despite geological and geodetic data suggesting the absence of linkage among the different en-echelon seismogenic faults in the L'Aquila area (e.g., Gori et al., 2012), a structural continuity has been proposed to explain the most recent seismological data (Falcucci et al., 2015). These faults are thought to have been coupled during several historical seismic sequences (e.g., Galadini & Galli, 2000; Galli et al., 2010, 2011; Vittori et al., 2011), generating different sized earthquakes, up to Mw 6.5–7.0 (Blumetti & Guerrieri, 2007; Storti et al., 2013).

3. Materials and Methods

We investigated the long-term evolution of the MPF through a multi-disciplinary approach that integrates fieldwork, mineralogical, geochemical, and geochronological analyses. The field surveys were carried out along the southwestern flank of Mount Pettino through geological mapping at the 1:10,000 scale (Figure 3). For the pre-orogenic carbonate substratum we refer to the stratigraphic scheme as provided by the Italian CARG (Geological CARtography) project (359-L'Aquila sheet; Centamore et al., 2006), whereas for the post-orogenic Pliocene-Quaternary deposits of the L'Aquila-Scoppito Sub-basin we referred to the geological maps of Nocentini et al. (2017, 2018). We built three geological cross-sections to understand the tectono-sedimentary architecture across the AIB. The main tectonic structures were identified by field surveys and remote analyses using a 10 m resolution LiDAR digital terrain model obtained from the open data portal of Regione Abruzzo, and a 1 m LiDAR DTM released by Friuli Venezia Giulia Civil Protection Institution. We investigated the structural architecture across the study area by collecting 367 structural measurements at 10 structural stops distributed along the fault traces, measuring fault strike, slickenline lineation, jointing and bedrock attitudes. Structural analyses along and across the main fault traces allowed to reconstruct fault geometry, architecture, and kinematics by measuring pitch and/or azimuth directions from syn-kinematic structures (i.e., abrasive striae and slickenfibers). Projection and statistical analyses of the structural data were performed through the Daisy.3 software (Salvini, 2019). Fault strikes and slickenline orientations were studied through statistical analyses and polymodal Gaussian fit frequency analyses to individuate the different distributions. The structural data set has been normalized by stations to avoid bias produced by the number of data of each station. Three main structural stops were selected as sampling sites to recover a total of 55 rock samples for carbonate isotopes analyses and geochronology. To investigate the origin and composition of the syn-tectonic fluids and their interactions within the MPF zone, we performed stable isotope analyses ($\delta^{13}C$, $\delta^{18}O$) and Δ_{47} (clumped isotopes) thermometry. XRD diffraction

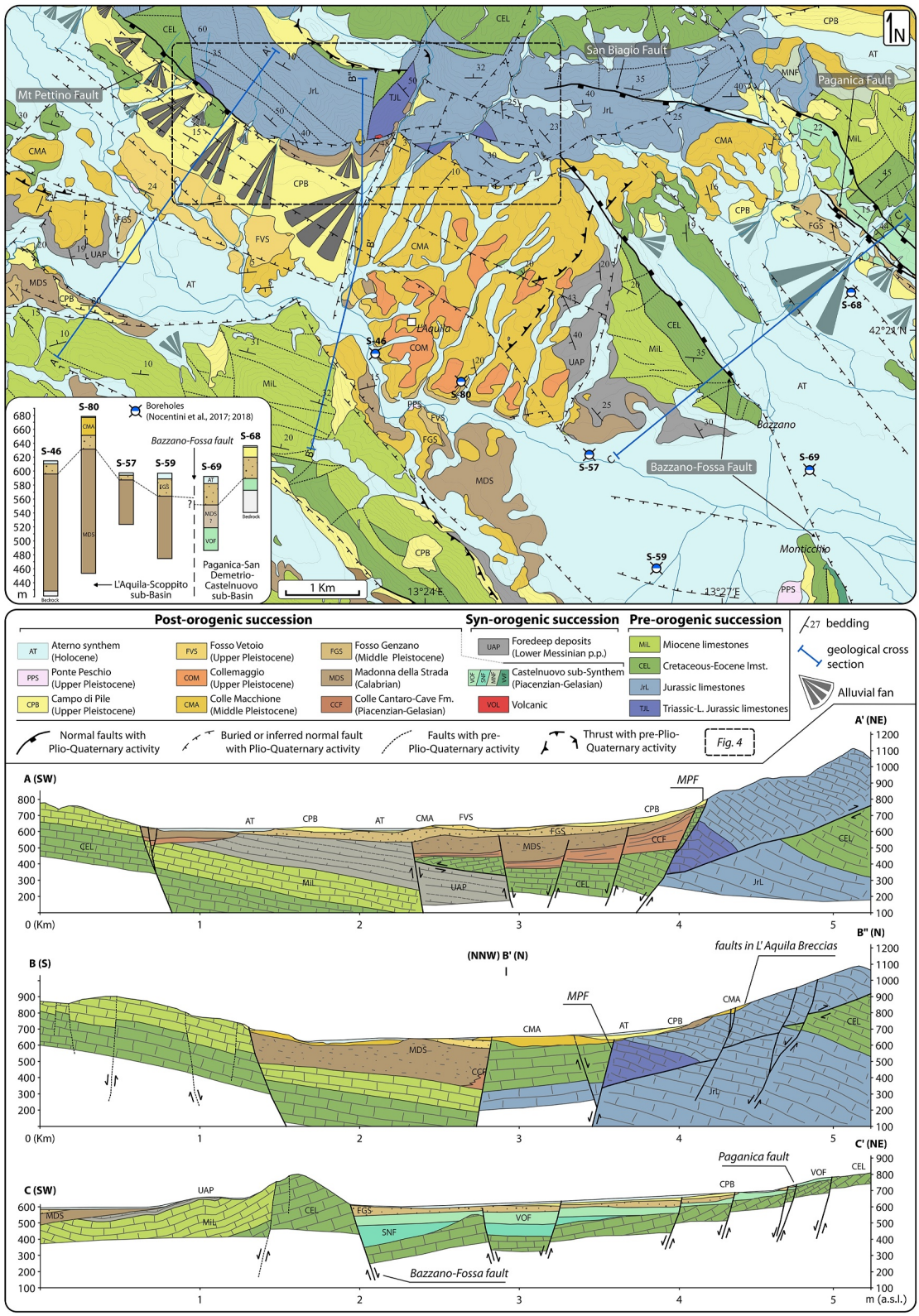

Figure 3. Geological map with boreholes stratigraphy (modified after Nocentini et al. (2017)) and geological cross-sections of the eastern portion of the ASB and the northwestern sector of the PSC, between Pettino and Paganica faults.

analyses were used to assess the mineral assemblage of the samples. To constrain the age of tectonic structures, we integrated carbonate U-Th (Cheng et al., 2013; Shen et al., 2012) and $^{40}Ar/^{39}Ar$ geochronological techniques. A list of the studied samples, their location, and the adopted analytical methods are provided in Table 1. Details of the analytical protocols and additional results are provided in Supporting Information S1.

4. Results

4.1. Structural Setting

Structural analysis focused on the central sector of the AIB, in the junction area between the basin boundary faults of the ASB and the PSC sub-basins (Figures 1a and 4a). Our surveys across the MPF have documented two distinct tectonic styles, characterized by different structural maturity of the fault zone and space distribution/localization, corresponding to the central portion of the MPF (Stops 1 and 2; Figure 4a) and to the overlay zone between the MPF and the PGF-SBF faults (Stops 3–9; Figure 4a), respectively.

The structure of the MPF is depicted by the A-A′ geological cross-section shown in Figure 3. The main exposure of the MPF is located at the piedmont of the SW flank of Mount Pettino, forming a 5–8 m-high tectonic scarp, with a NW-SE strike. It consists of a steeply dipping panel of cohesive cataclastic rocks (fault core), which is exposed for a length of ∼100 m, with a thickness ranging from 3 to 5 m. The cataclastic rocks separate fractured carbonate bedrock at the footwall from the Quaternary deposits described by Galli et al. (2010) at the hanging wall (see Section 4.1.1; Figure 5).

The fault core is characterized by the occurrence of sub-vertical synthetic Riedel shear surfaces showing dip-slip slickenlines (mainly abrasive striae) with normal slip. The contouring of pole to fault planes indicates a dominant NW-SE orientation, with a maximum concentration at N128°, 66° ($n = 41$, Figure 4b). Polymodal Gaussian fit distribution analyses identified two azimuthal frequencies of fault strikes; a main (81% of the data) orientation at N128° ± 8° (1SD) and a secondary one (19% of the data) oriented at N101° ± 5° (1SD), respectively (Figure 4b). Contouring of slickenlines on the fault planes shows a maximum concentration at N211°, 67° ($n = 35$), which corresponds to a pitch angle of 88°, documenting the dominant dip-slip kinematics along the MPF.

In the overlay zone between the MPF and the PGF-SBF, a newly discovered outcrop of faulted volcaniclastic deposit was recognized to unconformably cover the carbonate bedrock near the S. Giuliano Monastery (Figure 4a; see Section 4.1.3). An anastomosed array of extensional fault splays is recognized (Figure 4a), often arranged in conjugate fault systems (see stereoplots of Stop-3 and Stops-6-8; Figure 4a). The fault systems consist of NW-SE and E-W striking extensional fault strands, overprinting syn-orogenic NW-SE thrust faults and associated SW-NE striking strike-slip and oblique faults (Stop-3 in Figures 4 and 6a–6c). Contouring of pole to extensional fault planes ($n = 142$; Figure 4c) shows a maximum concentration at N127°, 68°, with a second concentration at N89°, 73° (Figure 4c). Polymodal Gaussian fit distribution analyses allow the identification of two main groups of fault azimuths, striking NW-SE (81% of the data; main at N123° ± 13°, 1 SD) and ca. E-W (19% of the data; main at N83° ± 8°, 1SD). The contouring of the slickenline distribution shows a main concentration at N185°, 75° ($N = 88$; Figure 4c). Extensional faulting affects the Middle Pleistocene deposits of the L'Aquila Breccia Fm., which unconformably cover the carbonate bedrock on the eastern flank of the Mount Pettino at different altitudes (Figure 4a), cropping out from ∼843–824 m (Figures 6b and 6d), up to 1,029 m a.s.l. (Figure 6e). The same deposits form a thick plateau around the L'Aquila Town, having the base at ∼650 m a.s.l. (Nocentini et al., 2017). Section D-D′ (Figure 6f) is constructed across these fault systems, showing a post-Middle Pleistocene cumulative vertical separation of ∼380 m, as calculated from the displaced outcrops of the L'Aquila Breccias Fm. Taking into account the dip angle of the Breccias (∼8°), using the available 1 m LiDAR digital elevation model of the study area, we estimate the vertical offset operated by main fault strands, with calculated displacements reaching up to approximately 76 and 101 ± 1 m, respectively (Figure 6f).

4.1.1. Sampling Site-1 (Stop-1): Fault Core of the MPF (Lat. 42°22′30.03″N, Long. 13°21′59.68″E)

Sampling site-1 corresponds to the exhumed fault core along the main trace of the MPF (Figures 4a and 5). The fault rocks consist of cemented and foliated, matrix-supported, cataclasite with a light gray color (Figures S1a and S1b in Supporting Information S1). The cataclasite includes grains of the carbonate host rock, with sub-rounded to well-rounded shape, from mm to cm in diameter (Figure S1c in Supporting Information S1). The XRD analyses indicated that the host rock grains and cataclasite matrix are made of dolomite/ankerite, with minor calcite (Table

10.1029/2024TC008548

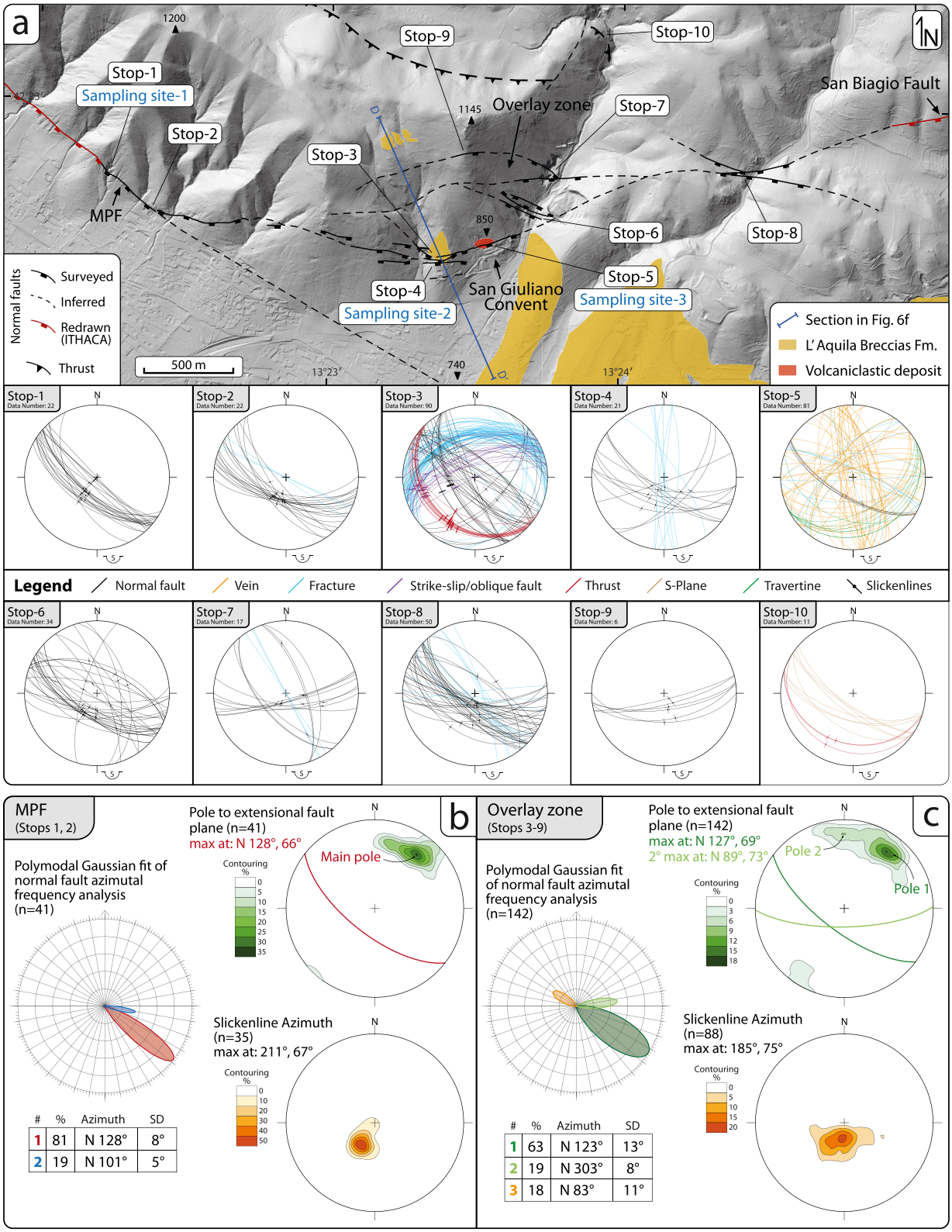

Figure 4. (a) Map of the tectonic structures surveyed in this work, with structural stops locations and stereographic projections (Schmidt net, lower hemisphere) of the structural data. (b, c) Statistical analyses utilizing Daisy.3 software (Salvini, 2019) of the main fault zone and the overlay zone, respectively. Each panel comprises the frequency distribution analyses of the faults strikes with polymodal Gaussian fit (left) and contouring of pole to fault plane (top-right) and slickenline attitudes (bottom-right).

Table 1
List of the 55 Samples and the Results of the Geochemical and Geochronological Analyses

Sample	Type	Sampling Site	Composition	$\delta^{13}C$ (V-PDB)	$\delta^{18}O$ (V-PDB)	T Δ_{47} (°C; ± SE)	Ar-Ar age (ka; ± 2σ)	U-Th age (yr BP; ± 2σ)
MPF-S1	Bedrock	1	Ankerite-Dolomite	1.12	−0.89			
MPF-S2	Bedrock	1	Ankerite-Dolomite	2.67	−0.23			
MPF5-M	Cataclasite matrix	1	Calcite- Ankerite-Dolomite	1.09	−1.81			
MPF5-U	Cataclasite gouge	1	Ankerite-Dolomite	2.56	−0.52			
MPF6-C1	Cataclasite clast	1	Ankerite-calcite	2.14	−1.3	42.4 ± 2.5		
MPF6-C3	Cataclasite clast	1	Ankerite-calcite	2.31	−0.44	33.1 ± 2.4		
MPF6-M1	Cataclasite matrix	1	Ankerite-calcite	−1.99	−1.16	44.0 ± 2.6		
MPF6-M2	Cataclasite matrix	1	Ankerite-calcite	1.71	−1.2	34.6 ± 2.5		
MPF6-M3	Cataclasite matrix	1	Ankerite-Dolomite	2.63	0.02			
MPF7-C1	Cataclasite clast	1	Ankerite-Calcite	−2.39	−1.35	50.2 ± 2.6		
MPF7-U1	Cataclasite gouge	1	Ankerite-Dolomite	0.71	−2.68			
MPF7-U2	Cataclasite gouge	1	Ankerite-Dolomite	1.14	−1.72			
MPF13-C	Cataclasite clast	1	Ankerite-Dolomite	2.37	−0.50			
MPF13-M	Cataclasite matrix	1	Ankerite-Dolomite	1.42	−1.40			
MPF14-C	Cataclasite clast	1	Ankerite-Dolomite	1.97	−2.09			
MPF14-M	Cataclasite matrix	1	Ankerite-Dolomite	1.01	−1.45			
MPF15-C	Cataclasite clast	1	Ankerite-Dolomite	2.18	−1.22			
MPF15-C	Cataclasite clast	1	Ankerite-Dolomite	2.26	−0.88			
MPF16-C	Cataclasite matrix	1	Ankerite-Dolomite	1.56	−0.55			
MPF25-U	Cataclasite gouge	1	Ankerite-Dolomite	1.82	−1.29	48 ± 4		
MPFS-3	Bedrock	2	Calcite	1.90	0.47			
MPFS-4	Bedrock	2	Calcite	1.93	2.01			
MPFB-1	Slickenfiber	2	Calcite	4.21	−1.19			
MPFB-2	Slickenfiber	2	Calcite	−10.35	−6.21			
MPFB-3	Slickenfiber	2	Calcite	−7.27	−6.86			
MPFS-5	Bedrock	3	Calcite	1.41	−0.12			
MPFS-6	Bedrock	3	Calcite	2.17	−0.07			
T-1	Travertine	3	Calcite	−7.63	−8.08	6.9 ± 1.9		>600
T-2	Travertine	3	Calcite	−10.09	−6.82			
T-3	Travertine	3	Calcite	−8.50	−6.67			
T-4	Travertine	3	Calcite	−9.90	−6.62			
T-5	Travertine	3	Calcite	−8.21	−6.45			331 ± 26
T-6	Travertine	3	Calcite	−9.68	−6.80			
T-7	Travertine	3	Calcite	−9.72	−6.11			
T-8	Travertine	3	Calcite	−8.80	−6.26			
T-9	Travertine	3	Calcite	−9.63	−6.54			233 ± 21
T-10	Travertine	3	Calcite	−8.76	−6.44			
T-11	Travertine	3	Calcite	−9.74	−6.55			
T-12	Travertine	3	Calcite	−9.79	−6.15			
V-1	Vein	3	Calcite	−8.37	−7.94	8.3 ± 1.9		182 ± 17
V-2	Vein	3	Calcite	−9.06	−7.06			
V-3	Vein	3	Calcite	−9.92	−6.58			

Table 1
Continued

Sample	Type	Sampling Site	Composition	$\delta^{13}C$ (V-PDB)	$\delta^{18}O$ (V-PDB)	T Δ_{47} (°C; ± SE)	Ar-Ar age (ka; ± 2σ)	U-Th age (yr BP; ± 2σ)
V-4	Vein	3	Calcite	−9.84	−6.36			
V-5	Vein	3	Calcite	−9.87	−6.43			
V-6	Vein	3	Calcite	−9.63	−6.02			–
V-7	Vein	3	Calcite	−9.57	−5.83			
V-8	Vein	3	Calcite	−10.47	−6.95			
V-9	Vein	3	Calcite	−9.79	−6.85			
V-10	Vein	3	Calcite	−9.88	−6.27			
V-11	Vein	3	Calcite	−9.68	−6.10			
V-12	Vein	3	Calcite	−9.59	−6.08			–
V-13	Vein	3	Calcite	−9.88	−6.17			
V-14	Vein	3	Calcite	−9.97	−6.30			
V-15	Vein	3	Calcite	−9.96	−6.36			
VOL-1	Volcanic deposit	3	Sanidine				416.88 ± 0.70	

Note. Samples with no analyses are left blank.

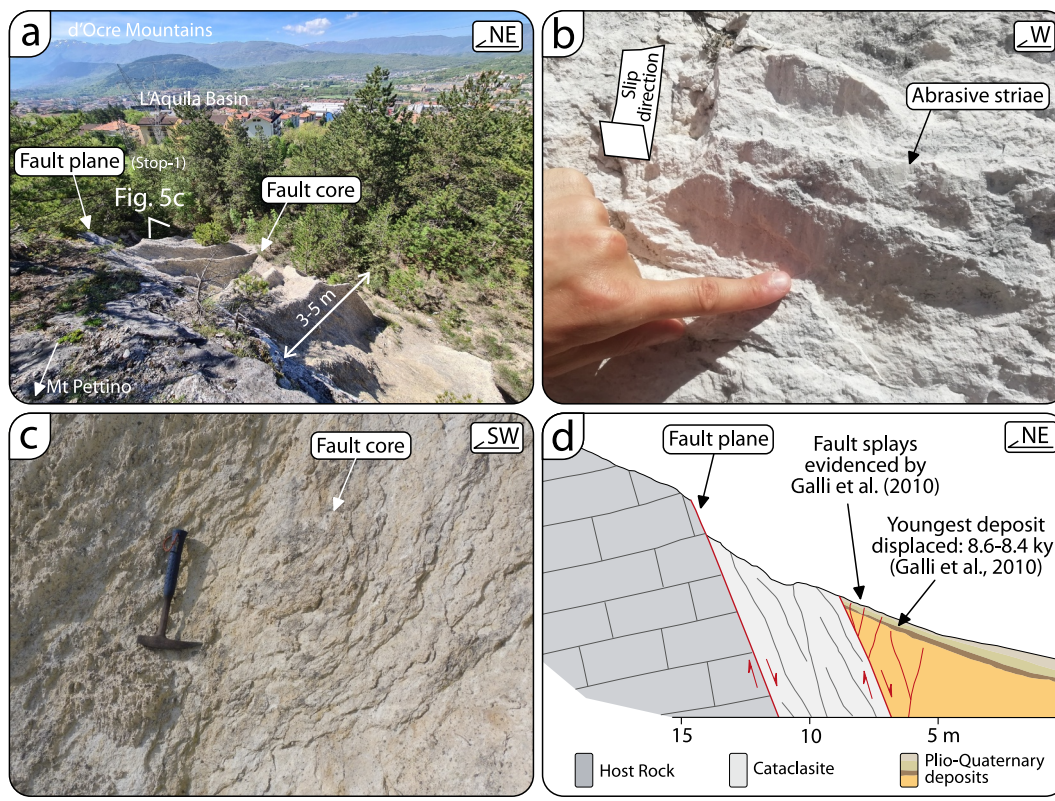

Figure 5. Sampling Site-1 (Stop-1; MPF main fault zone): (a) Panoramic view from the fault's footwall toward L'Aquila Basin showing a 3–5 m thick cataclastic fault core. (b) Detail of the fault surface with kinematic indicators (calcite steps and abrasive striae). (b) Side view of the foliated cataclasite forming the fault core. (d) Schematic representation of the outcrop (modified after Galli et al. (2011)).

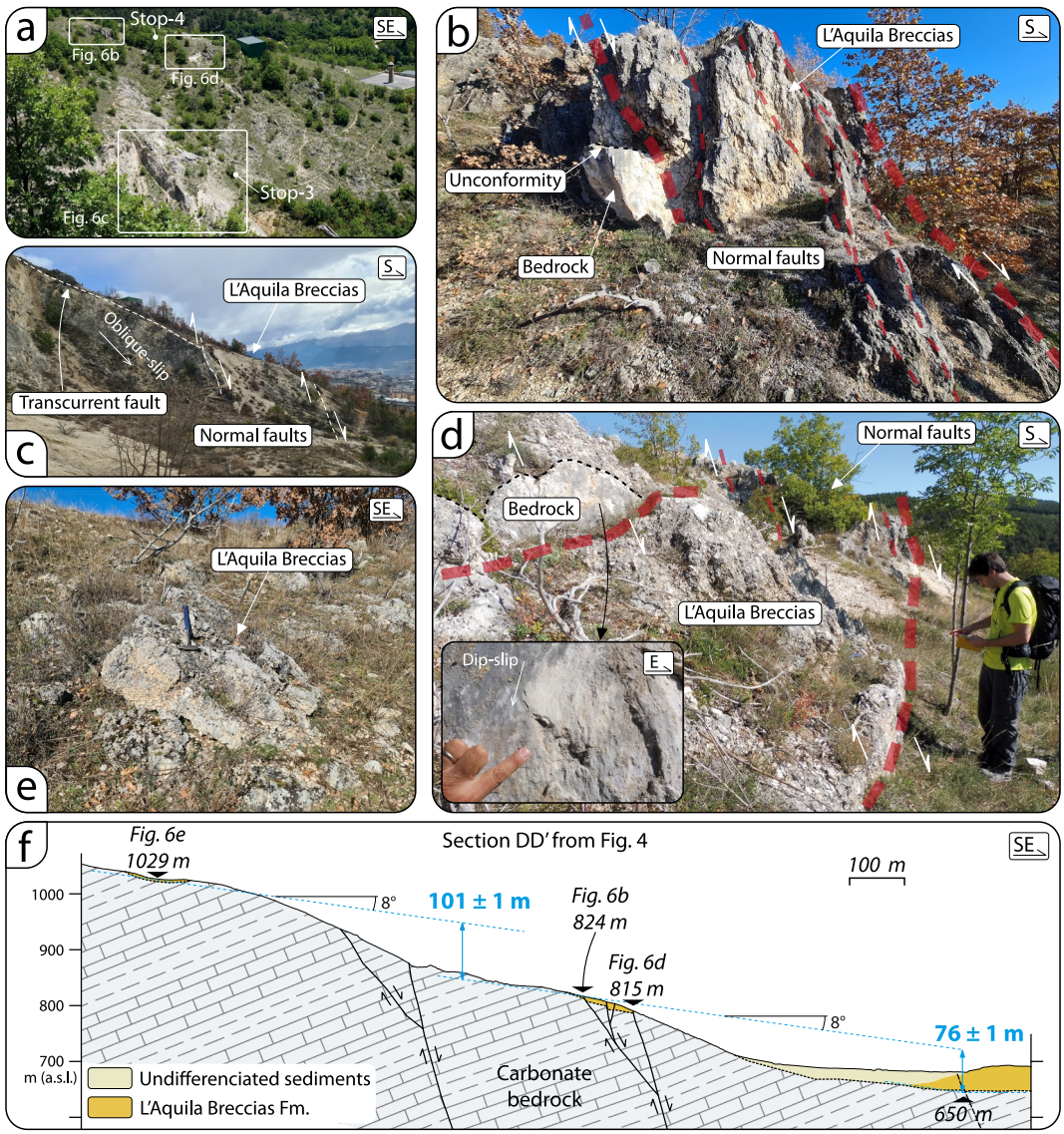

Figure 6. Sampling Site-2 (Stop-4; faults in L'Aquila Breccias Fm.; ca 350 ka): (a) Panoramic view of Stops 3 and 4 from Mount Pettino. (b) High angle extensional faults affecting the L'Aquila Breccias Fm. and the carbonate bedrock. (c) Normal faults overprinting an oblique-slip fault in the carbonate bedrock. The faults affect the L'Aquila Breccias Fm. (d) High angle extensional faults affecting the L'Aquila Breccias Fm. and the bedrock ~10 m below the outcrop shown in Figure 4c. The small panel shows the fault surface with dip-slip slickenlines (abrasive striae). (e) Outcrop of the L'Aquila Breccias Fm. toward the top of the Mount Pettino, at ~1,029 m of elevation. (f) Simplified geological cross section D-D′ (trace in Figure 4a), topography was built using the 1-m Lidar DTM.

S1 in Supporting Information S1). According to the classification proposed by Ferraro et al. (2018), the fault rock is dominantly composed of a matrix-supported cataclasite (Ms-type) with minor fine-grained white gouges (Fg-type). Samples of fault rocks (Ms- and Fg-type cataclasite), host rock grains and carbonate bedrocks were collected for $\delta^{13}C$, $\delta^{18}O$ stable isotopes and Δ_{47} (clumped isotopes) thermometry to investigate the fluid-rock interactions of the fault rocks (for details see Supporting Information S1).

4.1.2. Sampling Site-2 (Stop-4): Faults in the L'Aquila Breccias Fm. (Lat. 42°22′19.23″N, Long. 13°23′14.91″E)

The Sampling Site-2 is located north of the town of L'Aquila, where the L'Aquila Breccias unconformably rest on top of the carbonate bedrock from the piedmont (Figures 4a and 6). Structural investigations documented the presence of distributed high-angle normal faults, characterized by narrow fault cores (few mm to 1–2 cm), with spacing of up to some tens of meters. These fault structures define an anastomosed, WNW-ESE striking fault

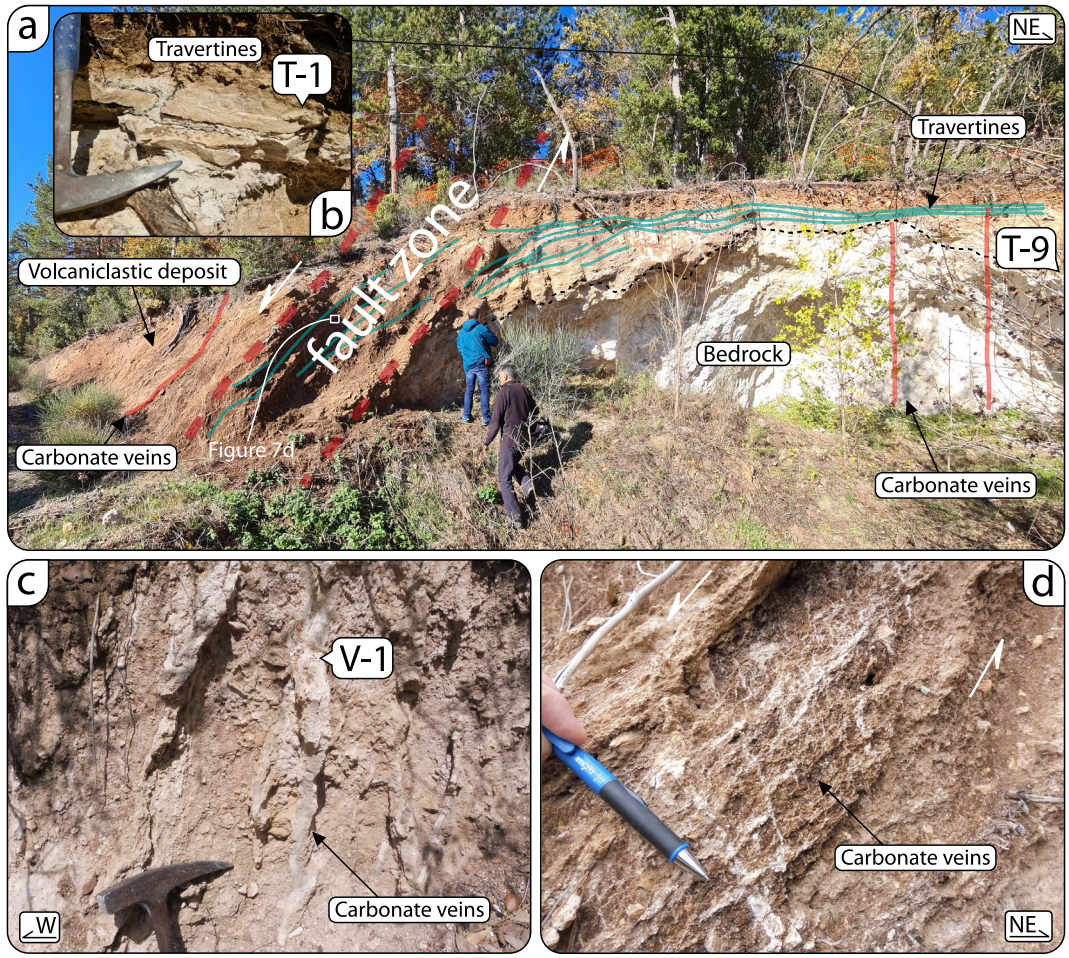

Figure 7. Sampling Site-3 (Stop-5; fault systems affecting the San Giuliano volcaniclastic deposits): T1, T9, and V1 are the carbonate samples (travertines and vein, respectively) investigated by U-Th geochronology (Table 2). (a) Panoramic view of the fault zone affecting the carbonate bedrock (fault footwall; to the right) and the overlying volcaniclastic deposits (fault hanging wall; to the left). The erosional contact is marked in the picture by a dashed black line. (b) Detail of the sampled travertine (T1). (c) Subvertical carbonate veins within yellowish continental deposits at the fault footwall. (d) Detail of the carbonate veins within the fault zone.

trace, dipping 60°–80° southward (Figures 6b and 6d). Calcite steps on fault plane show dip-slip kinematics and abrasive striae with a pitch angle ranging from 80° to 100° (Figure 6d). Fault slip on single fault segment varies from cm to m, as documented by the displacement of the base of the L'Aquila Breccias (Figures 6b–6d). Samples of calcite slickenfibers were collected from striated normal fault surfaces to investigate C-O systematics.

4.1.3. Sampling Site-3 (Stop-5): Faults Within the San Giuliano Volcaniclastic Deposit (Lat. 42°22′22.41″ N, Long. 13°23′26.71″E)

Close to the San Giuliano Convent, a ca. 10 m-thick reddish unconsolidated volcaniclastic deposit (detailed description of the mineralogical assemblage is reported in Figure S3 of the Supporting Information S1) unconformably rests above a yellowish continental colluvium and the carbonate substratum (Figure 7a). Stratified, sub-planar travertine bodies occur on top of the bedrock and embedded within the continental colluvium (Figures 7a and 7b). Their attitude is sub-parallel to the slope, dipping 20–25° toward SSE. This outcrop is characterized by intense brittle faulting and fracturing. A major fault zone is recognized to affect the volcaniclastic deposits, the colluvium, and the travertines. The fault surfaces strike E-W to NW-SE, dipping 30°–65° toward S-SW, showing normal offset (Figure 7a). The fault zone is decorated by diffuse carbonate veining (Figure 7d), with different geometries and relationships with the fault zone between the fault hanging wall and

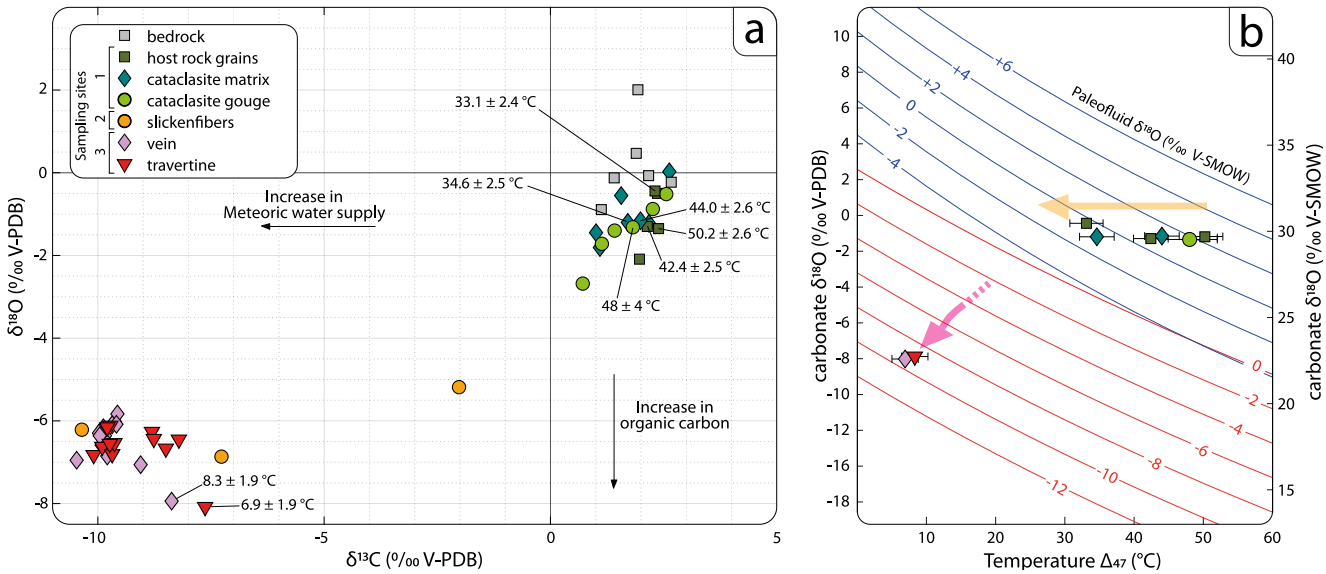

Figure 8. (a) Distribution of $\delta^{13}C$ and $\delta^{18}O$ of the carbonate samples collected in this work (‰ vs. V-PDB) with estimated temperatures (Δ_{47}). Carbonate bedrock samples (gray) resemble the mean isotopic values of the shallow-water carbonates in the central Apennines (Ghisetti et al., 2001). Samples from the MPF (Sampling Site-1; green) are mostly equilibrated with the carbonate bedrock (with a minor shift in $\delta^{18}O$) which would appear to be the main oxygen and carbon reservoir for the fluids that circulate within the fault zone. The tectonic structures in L'Aquila Breccias (Sampling Site-2; orange) and in the San Giuliano volcaniclastic deposit (Sampling Site-3; purple and red) show strong atmospheric water contamination, suggesting that syn-kinematic calcite has been precipitated in an open fluid circulation system, that interacted near the surface with meteoric water (e.g., Sharp, 2017). Temperatures obtained with clumped isotope analyses are plot in correspondence of the relative samples with the error as 1SE. (b) Distribution of the oxygen isotope composition ($\delta^{18}O$ ‰ vs. V-SMOW and V-PDB) versus temperature (Δ_{47}) of the eight carbonate samples analyzed with clumped isotopes. Paleofluid compositions have been calculated using the equation provided by Sheppard and Schwarcz (1970) for dolomite samples and by Kim and O'Neil (1997) for calcite samples.

footwall. The veins at the footwall of the fault are subvertical and reach up to 10 cm in thickness, spaced from a few cm to m (Figure 7c). These veins are distributed across the entire outcrop, forming a systematic array, with a main NNW-SSE orientation (Figures 7a and 7b). They show a whitish travertine laminated texture. At the fault hanging wall, the carbonate veins are concentrated within the fault zone (Figure 7d). These veins, up to 1–4 cm thick, form a non-systematic array, striking both sub-parallel and sub-perpendicular to the fault planes. Some of these veins accommodated minor tectonic slip that resulted in displacements of a few centimeters (Figure 7d). We collected several samples of carbonate veins and travertines for stable and clumped isotopes analyses (Table 1; Figure 8), as well as three samples of veins and three samples of travertine for U-Th analyses to indirectly constrain the age of tectonic activity. The veins and travertines are entirely composed of calcite (Table S1 in Supporting Information S1). Furthermore, sanidine crystals were separated from the volcaniclastic deposit (VOL-1 sample) to perform $^{40}Ar/^{39}Ar$ geochronology and constrain the age of the volcanism (Supporting Information S1 and Data Set S1; Table 1).

4.2. $\delta^{13}C$, $\delta^{18}O$ Stable Isotopes and Δ_{47} (Clumped Isotopes) Thermometry

The bedrock is characterized by $\delta^{13}C$ values ranging between 1.12 and 2.67‰ (note that ‰ values are given as deviation from V-PDB standard) and $\delta^{18}O$ values between −0.89 and 2.01‰ (Figure 8a). The isotopic composition of the fault-related structures from the MPF (Sampling Site-1) almost overlaps that of the carbonate bedrocks. Indeed, the cataclasite matrix, gouge and host rock grains have $\delta^{13}C$ values ranging from 0.71 to 2.63‰ and $\delta^{18}O$ values ranging from 0.02 to −2.68‰ (Figure 8a and Table 1). Results from fault slickenfibers collected within the L'Aquila Breccias (Sampling Site-2) display a wide range in the $\delta^{13}C$ isotopic compositions, spanning from −10.35 to −2.02‰, whilst the $\delta^{18}O$ values are in the range of −5.18 and −6.86‰. The veins and travertines associated with the fault zone at the Sampling Site-3 show consistent low $\delta^{13}C$ and $\delta^{18}O$ values, ranging from −7.36 to −10.46 and −5.83 to −8.08‰, respectively.

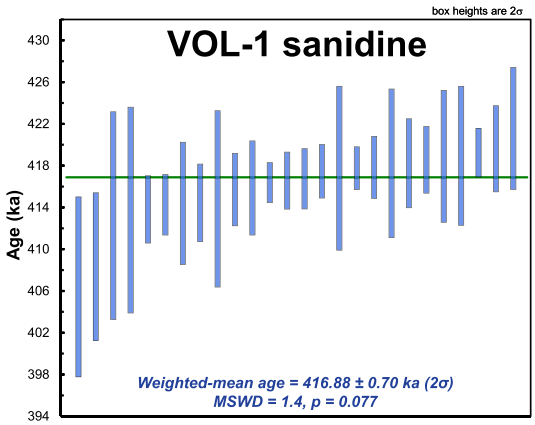

Figure 9. $^{40}Ar/^{39}Ar$ apparent ages and weighted-mean calculation for sanidine single grain fusion analyses ($n = 26$) from sample VOL-1. See details in Data Set S1.

The Δ_{47} value of the host rock grains (samples MPF6-C1, MPF6-C3, and MPF7-C1) is between 0.528 and 0.571‰ (I-CDES), whilst the cataclasite matrix (samples MPF6-M1 and MPF6-M2) ranges between 0.543 and 0.567‰ (I-CDES) and the fault gouge is 0.533‰ (I-CDES). The Δ_{47} of the carbonates in Sampling Site-3 (samples T1 and V1) is around 0.648–0.652‰ (I-CDES). Details and data set are available in Data Set S2.

Temperatures are calculated with the equation from Anderson et al. (2021) using the measured Δ_{47}. The cataclasite carbonates from the MPF (Sampling Site-1) show the highest temperature, with the cataclasite clasts having temperature ranging between 33 ± 2.4 and 50 ± 2.6°C (1 SE), whereas the cataclasite matrix are between 34.5 ± 2.4 and 44 ± 2.8°C (1 SE; Figure 8). One sample of fine-grained fault gouge provides a temperature estimate of 48 ± 4°C (1 SE). On the other hand, veins and travertines from Sampling Site-3 show lower temperature estimates, ranging between 6.9 ± 1.9 and 8.2 ± 1.9°C (1 SE).

The oxygen isotopic composition of the paleofluids was calculated using the measured temperature (Δ_{47}) and the equation by Sheppard and Schwarcz (1970), for dolomite compositions, and by Kim and O'Neil (1997) for calcite compositions, expressed in ‰ versus V-SMOW Figure 8b. The $\delta^{18}O$ composition of the paleo fluids with respect to the cataclasite matrix of the MPF varies from −0.8 to +1.2‰ ($n = 2$), for the host rock grains between 4 and 5‰ ($n = 3$), while for the fault gouge is ca. +1.8‰ ($n = 1$). $\delta^{18}O$ composition of the paleofluids related to travertine and vein ranges from −9 to −9.5‰ (Figure 8b).

4.3. Geochronology

4.3.1. $^{40}Ar/^{39}Ar$ Geochronology of the Volcaniclastic Deposit

Hand-picked sanidine grains from the San Giuliano volcaniclastic deposit (sample VOL-1) were selected after sample crushing and sieving (125 and 250 μm). The sanidine grains show single grain total fusion ages ranging from 225 ± 4 (one grain) to 480 ± 6 ka (2σ), although most of the grains yield ages in the range 413 ± 10 to 420 ± 4 ka (2σ; Figure 9). Given the spread in data, prior to calculation of a weighted-mean age, the data were filtered using a normalized median absolute deviation (nMAD) cut-off value of 3 (Powell et al., 2020), an approach that has been used in other Ar-Ar dating studies (e.g., Niespolo et al., 2017; Phillips et al., 2022; Rivera et al., 2013). Post-filtering, 26 grains were used to calculate a weighted-mean age of 416.88 ± 0.70 ka (2σ; MSWD = 1.4, $p = 0.077$; Figure 9) that can be considered as the emplacement age for sample VOL-1.

4.3.2. U-Th Carbonate Geochronology

U-Th carbonate dating was used to constrain the age of six structurally controlled carbonate structures (veins) and sub-horizontal carbonate concretions involved in the fault movement (travertines) at Sampling Site-3. The results are listed in Tables 1 and 2. ^{238}U concentration ranges from 381 to 1,114 ppb, while ^{232}Th concentration is comprised between 20.99 and 761 ppb. $^{230}Th/^{238}U$ activity ratio ranges from 0.9 to 1.4 and the $^{230}Th/^{232}Th$ Atomic ratio of five out of the six samples is between 14 and 18 × 10^{-6}, except for one sample (T1), which exceeds 987 × 10^{-6}. Overall U-Th geochronology returned ages falling in the late Middle Pleistocene (Chibanian), ranging between 182 and 331 ka. For two veins the measurement failed. For travertine (T1), the age is beyond the limits of the U-Th technique (~600 ka). Two travertines, samples T5 and T9 provided ages of 331 ± 26 and 233 ± 21 ka, respectively. Only one carbonate vein was successfully dated and provided the youngest age of 182 ± 17 ka.

5. Discussion

5.1. Tectonic Synthesis

Two distinct tectonic stages (Stage-1 and Stage-2), separated by periods of stasis and erosion were identified along the trace of the MPF. These tectonic stages are characterized by different structural maturities, deformation styles, and geochemical signatures, which vary along the strike of the faults.

Table 2
U-Th Isotopic Compositions and Ages of Carbonate Structures From Sampling Site-3

Sample ID	Carbonate type	^{238}U 10^{-9} g/g[a]	^{232}Th 10^{-9}g/g	$\delta_{234}U$ measured[a]	$[^{230}Th/^{238}U]$ activity[b]	$^{230}Th/^{232}Th$ atomic ($\times10^{-6}$)	Age (ka) uncorrected	Age (ka) corrected[b,c]	$\delta^{234}U_{initial}$ corrected[d]
T1	Travertine	1,114 ± 1	0.0210 ± 0.0001	92 ± 1	1.129 ± 0.005	988 ± 6	>600	>600	
T5	Travertine	506.4 ± 0.6	0.5 ± 0.1	49 ± 1	1.03 ± 0.01	18 ± 3	356 ± 27	331 ± 26	126 ± 10
T9	Travertine	769.3 ± 0.6	0.8 ± 0.3	28.7 ± 0.9	0.94 ± 0.01	16 ± 6	261 ± 12	233 ± 21	55 ± 4
V1	Vein	545.3 ± 0.5	0.5 ± 0.1	47 ± 1	0.905 ± 0.006	15 ± 2	210 ± 5	182 ± 17	79 ± 4
V6	Vein	383.1 ± 0.4	0.6 ± 0.1	31 ± 1	1.24 ± 0.02	14 ± 3	–		
V12	Vein	381.8 ± 0.5	0.7 ± 0.2	33 ± 1	1.40 ± 0.02	12 ± 3	–		

Note. Analytical errors are 2σ of the mean. [a]$[^{238}U] = [^{235}U] \times 137.818$ (±0.65‰) (Hiess et al., 2012); $\delta^{234}U = ([^{234}U/^{238}U]_{activity} - 1) \times 1{,}000$. [b]$[^{230}Th/^{238}U]_{activity} = 1 - e^{-\lambda230\ T} + (\delta^{234}U_{measured}/1{,}000)[\lambda_{230}/(\lambda_{230} - \lambda_{234})](1 - e^{-(\lambda230-\lambda234)\ T})$, where T is the age. Decay constants of ^{230}Th, ^{234}U, and ^{238}U are available in Cheng et al. (2013). [c]Age (ka) corrections, relative to chemistry date on 1950 CE, were calculated using an estimated atomic $^{230}Th/^{232}Th$ ratio of 4 (±2) × 10^{-6}. Those are the values for a material at secular equilibrium, with the crustal $^{232}Th/^{238}U$ value of 3.8. The errors are arbitrarily assumed to be 50%. [d]$\delta^{234}U_{initial}$ corrected was calculated based on ^{230}Th age (T), that is, $\delta^{234}U_{initial} = \delta^{234}U_{measured} \times e^{\lambda234\ T}$, and T is corrected age.

Stage-1 (Figure 10a) corresponds to the formation of a fault zone at the piedmont of the Mount Pettino, oriented NW-SE, consistent with the regional extension direction of the central Apennines (SW-NE). The fault zone comprises a rather thick (up to 5 m), foliated, matrix-supported cataclasite and a poorly developed damage zone at the transition to the carbonate bedrock. Isotopic analyses of the cataclastic fault rocks at Sampling Site-1 show rock buffered compositions (Eiler, 2011; Passey & Henkes, 2012) nearly equilibrated with the carbonate substrate. The $\delta^{13}C$ values of the carbonate rocks in the MPF cataclasite (matrix, clasts and gouge) range between 1 and 3‰, similar to those observed for the carbonate host rocks (Figure 8a), whose composition resembles that of shallow-water carbonates in the central Apennines (Ghisetti et al., 2001). This suggests that the host rocks represent the main C-source for the MPF cataclasite. The $\delta^{18}O$ values are instead slightly depleted of approximately 1–1.5‰ compared to the carbonate host rock (Figure 8a), hinting at the possible presence of deep/connate fluids infiltrating within the fault zone (e.g., Kirkwood et al., 2001; Smeraglia et al., 2016). However, the observed shift is very small compared to what observed in Smeraglia et al. (2016). Indeed, the MPF cataclasite appears to be an almost-closed geochemical system, suggesting that even if burial fluids circulated within the fault zone, they had little effect. Intriguingly, no isotopic signature of meteoric water was found. This evidence indicates that the MPF cataclasite did not interact with surface water circuits during its development and therefore represents an exhumed fault zone (Figure 10a). This is also confirmed by T (derived from Δ_{47}) estimated for the cataclasite matrix and fault gouge, ranging between 35 and 50°C. These estimates appear too warm to reflect rainwater temperatures. The calculated paleofluids compositions allow the determination of a shift in the $\delta^{18}O$ composition of the precipitating fluid (in ‰ vs. V-SMOW) of ∼3‰ with the decrease in precipitating temperature (Figure 8b). Interestingly, this evidence might indicate a fluid evolution to colder conditions during stage-1 faulting, and hence during the fault zone exhumation. The nature of the cataclastic rocks (governed by comminution) makes it challenging to interpret the meaning of these temperature estimates, which may reflect a combination of pre-tectonic events, such us diagenetic mineral growths and complex T-t history (e.g., Huntington & Petersen, 2023; Nooitgedacht et al., 2021). However, assuming that the peak temperatures are indicative of the thermal conditions of deep/connate fluids involved in the early stages of faulting (Curzi, Aldega, et al., 2024; Smeraglia et al., 2016), and considering a geothermal gradient of 24°C/km (Diaferia et al., 2019), we infer a depth of exhumation for the cataclastic fault rocks of the MPF ranging between 1.4 and 2.1 km. This inference is consistent with the vertical offset of the MPF (1.5–2 km, see also Iezzi et al. (2019)).

In general, exhumation of the footwall block due to normal faulting at shallow crustal levels is typically influenced by the concurrent action of tectonic processes and erosion (Ring et al., 1999). In continental settings, such as the central Apennines, erosion is mostly driven by river incision. As demonstrated by Nocentini et al. (2017), the amount of river incision inside the AIB is relatively low, as the elevation of the oldest fluvial deposit terraces (Fosso Genzano Fm.) across the entire basin is approximately 40 m above the present-day river altitude. This indicates an incision rate in the hanging wall sector of the MPF in the order of 0.05–0.07 mm/yr during the last 0.8–0.6 Ma. Furthermore, between 3 and 1.1 Ma, the AIB was characterized by an internally drained fluvial

10.1029/2024TC008548

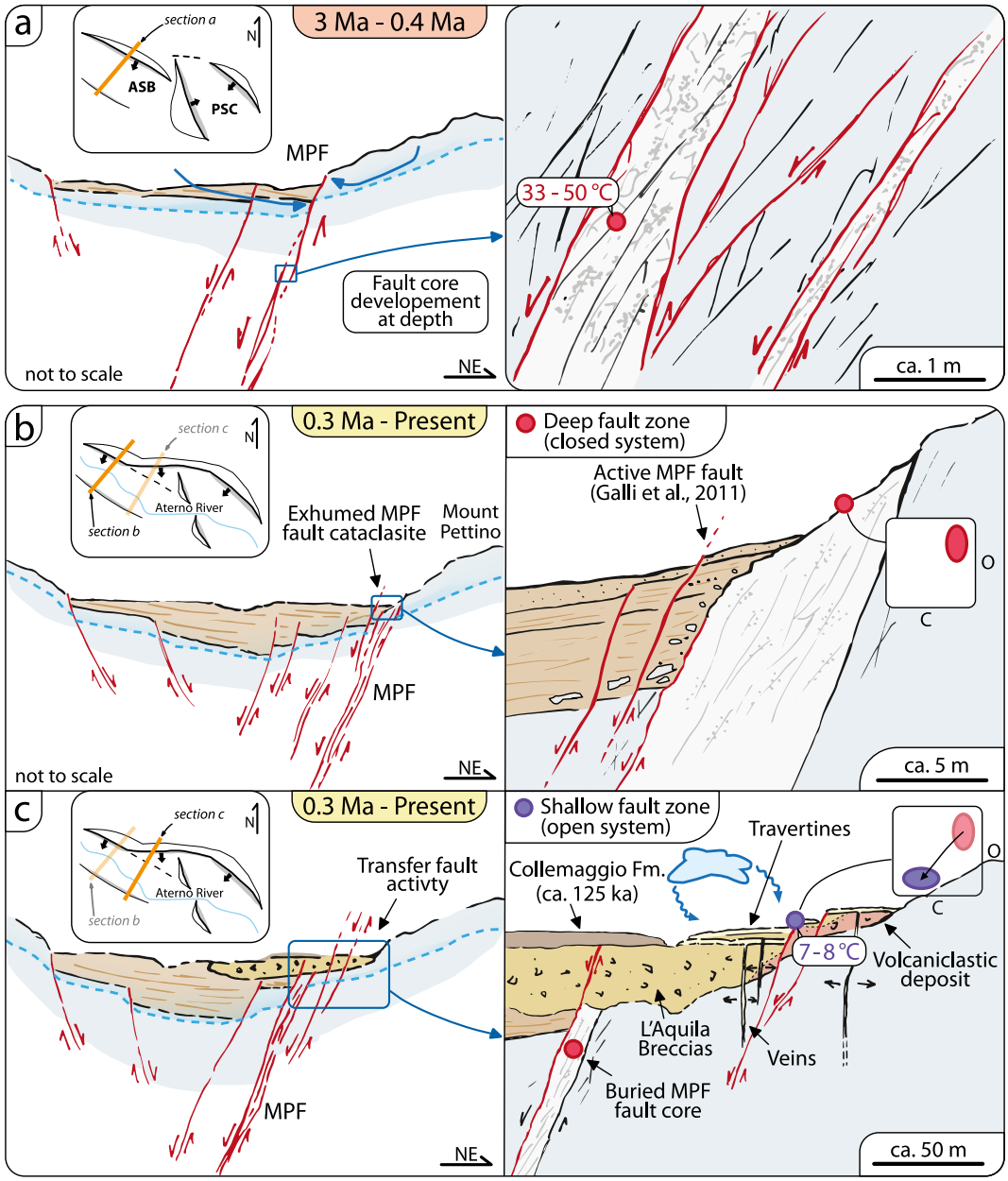

Figure 10. Schematic evolution of the MPF through time (location of structures is only indicative). (a) Stage-1 faulting, occurring since the Late Pliocene when the basin boundary fault started developing at depth, and lasted until its exhumation, constrained (at least) before the deposition of the oldest deposits, which are represented by the volcaniclastic deposit of the San Giuliano convent (~0.4 Ma). Development of the fault core occurred in a closed geochemical system that did not involve the interaction with meteoric fluids, with temperatures (Δ_{47}) of 33–50°C. Assuming that these values correspond to the equilibrium temperatures of deep/connate fluids circulating within the fault zone at depth, this might indicate a depth of formation of ~1.4–2.1 km (considering a geothermal gradient of 24°C/km, Diaferia et al., 2019). Panels (b and c) both refer to stage-2 faulting but are sections in two different locations. (b) Stage-2 faulting depicted in the central portion of the MPF, where evidence of Stage-1 faulting is exhumed due to hanging wall downfaulting generated by continuous tectonic activity (still active) localized at the piedmont of the Mount Pettino (Galli et al., 2011). (c) Stage-2 faulting in the SE sector of the MPF, where the cataclasite of the Stage-1 is covered by the L'Aquila Breccias Fm. and extensional deformation progressively vanished. Faulting localized in the transfer zone between MPF and the PGF-SBF, cutting across the L'Aquila Breccias Fm. (~350 ka) and the San Giuliano volcaniclastic deposits (416.88 ± 0.70 ka). Tectonic activity is constrained between 182 and 331 ka during deposition of carbonates with temperature (Δ_{47}) close to groundwater values (7–8°C).

system, which indicates that the fluvial incision was markedly low (Geurts et al., 2020). Given the negligible contribution of erosion estimated by the low rates of river incision, we infer that the exhumation registered by the cataclastic core of the MPF was mostly tectonically driven.

Stage-2 is documented by faults affecting the hanging wall of fault rocks of the MPF (Galli et al., 2011; Figure 10b) and by the tectono-stratigraphic setting in the overlay zone between the MPF and PGF-SBF (Stops 3–9; Figure 4a), where tectonic structures exhibit delocalized brittle deformation with poorly developed and anastomosed fault segments (Figure 10c). The overlay zone corresponds to a region of intense fluid-rock interaction and carbonate mineralization, assisted by faulting and fracturing. Indeed, transfer zones between faults represent areas associated with increased secondary permeability, serving as conduits for structurally controlled fluid circulation (Childs et al., 1995; De Paola et al., 2007; Fossen & Rotevatn, 2016; Larsen, 1988; Morley et al., 1990; Peacock & Sanderson, 1991), as documented by diffuse carbonate veining and travertine deposition (Brogi et al., 2021; Kim & Sanderson, 2010). Isotopically, these carbonate structures show strongly negative $\delta^{13}C$ and $\delta^{18}O$ values, indicating a trend toward a depleted carbon and oxygen source (Figure 8). The oxygen values of the carbonate samples (travertines and veins), ranging from −6 to −8‰ (V-PDB), indicate a dominant contribution of meteoric water, with values consistent with the local rainwater isotopic composition (San Jose et al., 2020), as well with the isotopic water composition of carbonate aquifers in the central Apennines (Falcone et al., 2008). The depleted $\delta^{13}C$ values (−8 to −10‰ vs. V-PDB) indicate the imprinting of organic-derived carbon (Sharp, 2017) (Figure 8a), suggesting that parental fluids circulated in organic rich soils before precipitating. Moreover, clumped isotopes analyses provide temperature estimates for the vein and travertines of 7–8°C, which are consistent with the temperature measured on groundwater in the area (Falcone et al., 2008). This evidence indicates precipitation of syn-kinematic authigenic carbonates (veins) and the associated travertine depositions as occurred in an open fluid circulation system near the surface, in contact with meteoric water that infiltrated the fault zones during tectonic activity (Figure 10c). This scenario deviates from the closed system documented in Stage-1, suggesting that the tectonic activity occurred after the exhumation of the fault core cataclasite. Moreover, in this region, the MPF cataclasite is buried below the continental deposits of the L'Aquila Breccias Fm. These breccias formed about 350 kyr ago from a debris avalanche in the Gran Sasso area (Cosentino et al., 2017, and references therein). The age of 416.88 ± 0.70 ka obtained from the volcaniclastic deposit further confirms the scenario of the MPF fault zone exhumation before the Middle Pleistocene.

Interestingly, the Stage-2 structures suggest that fault activity operated by breaching faults connecting the basin boundary faults of the AIB via hard linkage (Cartwright et al., 1995; Gibbs, 1984; Peacock et al., 2000; Walsh & Watterson, 1991; Walsh et al., 2003) between the MPF and the PGF-SBF. In this scenario, the Stage-2 faulting reflects the structural connections among the different extensional faults of the rift, which tends to evolve toward more mature stages (e.g., Cowie & Scholz, 1992; Hus et al., 2006; Peacock & Sanderson, 1991; Trudgill & Cartwright, 1994; Walsh & Watterson, 1991; Zwaan et al., 2016). The structural connection was primarily accommodated by NW-SE oriented (sub-parallel to the MPF strike) associated with E-W oriented extensional faults (Figure 4c). The frequency distribution analysis of the slickenlines of the extensional faults indicates a N-S oriented (N185°, 75°) maximum extension direction (Figure 4c), indicating a deviation with respect to the main regional direction (NE-SW) which typically occurs in transfer zones to accommodate the fault linkage (e.g., Acocella et al., 1999). Indeed, relay zones are areas characterized by intensive fracturing caused by twisting and rotation of tectonic blocks, which can create deformation patterns that can also differ from the far field stress regime (Peacock & Sanderson, 1991). The U-Th ages of the carbonate veins at Sampling Site-3 allow us to propose that the hard linkage between the MPF and the PGF-SBF was active, at least, between 182 and 331 kyr.

5.2. Estimate of the Long-Term Slip Rates

The highest offset of the Late Pliocene-Quaternary normal faults can be used to estimate the maximum long-term slip rate of these faults during the time frame of their activity (e.g., Blumetti & Guerrieri, 2007; Pizzi et al., 2002; Roberts & Michetti, 2004), on the assumption that the fault throw was produced exclusively during the active extensional tectonic phase. Considering a vertical displacement of 1.5–2 km accumulated in the last 3 Myr by the MPF, it results in a maximum long-term slip rate of 0.50–0.67 mm/yr (Figure 11). Long-term estimation does not allow for the identification of potential changes in fault activity over time. This is because such methods tend to smooth the slip rate, thereby obscuring any possible variation. It is reasonable to assume that the MPF may have experienced variations in fault kinematics over time, due to changes in the regional stress or local factors (e.g., Galadini, 1999; Lanari et al., 2021; Roberts & Michetti, 2004). However, it is interesting to note that this long-term estimate is (a) very close to the Holocene slip rate of 0.6 mm/yr as proposed by Galli et al. (2011), and (b) compatible with the estimated slip rate of 0.47–0.86 mm/yr for the last 31 kyr by Galadini and Galli (2000)

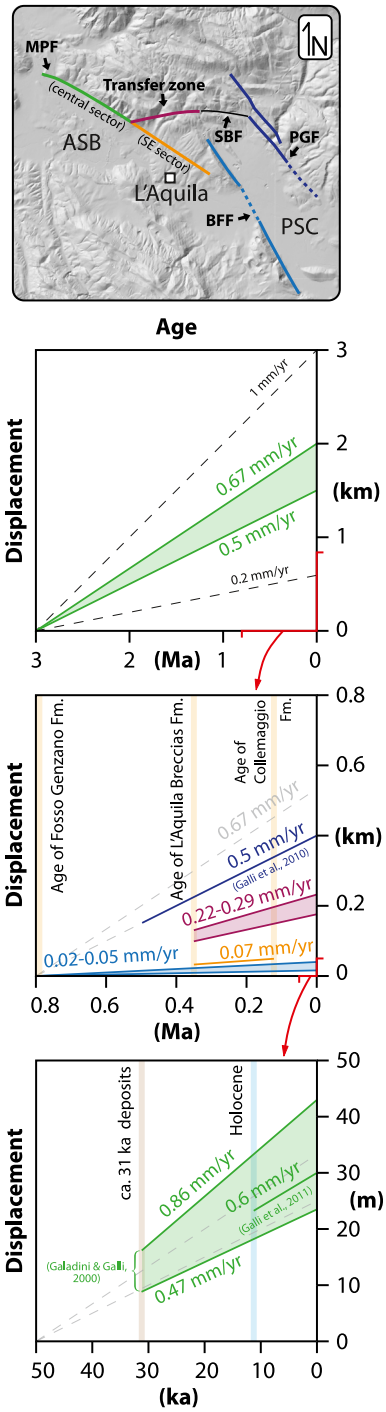

Figure 11. From top to bottom: Map (upper panel) of the main basin boundary faults of the L'Aquila Intermontane Basin (ASB: L'Aquila-Scoppito Sub-basin; PSC: Paganica-San Demetrio-Castelnuovo Sub-basin, with the corresponding long- to short-term fault slip rates over the last 3 Ma, as estimated in this work and from literature (lower panels). The different colors refer to each fault as depicted in the map (top frame); green: MPF (central sector); orange: MPF (SE sector); purple: Transfer zone; dark blue: PGF; light blue: BFF. Dashed lines are inferred or buried faults. See main text for details.

(Figure 11). This similarity allows for the reasonable speculation that, over the long-term, the central sector of the MPF likely moved with a constant slip for the last 3 Ma, until the present.

In contrast, over the past 350 kyr, the southeastern portion of the MPF, in correspondence of L'Aquila town, has exhibited a slip rate of 0.07 mm/yr, indicating a reduction in the slip rate by 90% when compared to its central sector, at least since the deposition of the L'Aquila Breccias Fm. (Figure 11). This is also corroborated by the sealing of the fault by the Upper Pleistocene (~125 ka) deposits of the Collemaggio Fm. (Nocentini et al., 2017; Tallini et al., 2019). A comparable scenario is observed to the south, in the Bazzano-Fossa normal fault, the western basin-boundary fault of the PSC. In-depth correlation of the Fosso Genzano Fm. deposits across the fault reveals a vertical offset between 15 and 43 m over the past 0.8 Myr (Figure 11). This evidence suggests that the maximum long-term slip rate of the BFF is between 0.02 and 0.05 mm/yr, which corresponds to 4%–11% of the slip rate of the antithetic Paganica Fault (0.44–0.5 mm/yr; Puliti et al., 2022; Galli et al., 2010). On the other hand, in the overlay zone between the MPF and the PGF-SBF, several fault splays (Stage-2 faulting) affect the L'Aquila Breccias Fm., with a total vertical displacement of ~76 and 101 ± 1 m, respectively, along the main fault strands. Based on the stratigraphic age of the faulted deposits (~350 ka; Cosentino et al., 2017), we obtain a cumulative slip rate spanning ~0.22–0.29 mm/yr (Figure 11). Correlation of not originally sub-horizontal deposits (such as the rock-avalanche deposits of the L'Aquila Breccias Fm.) might have caused a slight overestimation of the vertical fault offset and, consequently, in the slip-rate, which would be thus considered as a maximum long-term slip rate during Stage-2 faulting. Nevertheless, our results suggest that the slip rate of the overlay zone efficiently operated as a transfer zone between the MPF and the PGF-SBF at least from the Middle Pleistocene.

5.3. Tecto-Stratigraphic Evolution of the AIB

The depositional systems in extensional basins are controlled by the space-time activity of the basin boundary faults. Many studies emphasize how tectonic interaction and connection of fault segments play a fundamental role in the stratigraphic evolution of the basins (Gawthorpe & Hurst, 1993; Gupta et al., 1998; Larsen, 1988). The early stages of extensional basins are typically characterized by endorheic drainage systems, which evolve to exorheic drainage via long-term river drainage integration, as a consequence of the progressive development of basin boundary faults within a rift system (D'Agostino et al., 2001; Duffy et al., 2015; Gawthorpe & Leeder, 2000; Geurts et al., 2018). A pivotal role in the tectono-stratigraphic evolution is played by the transition from soft- to hard linkage of basin boundary fault segments during rift propagation (e.g., Gawthorpe & Leeder, 2000). During the Gelasian-early Calabrian, the ASB and PSC sub-basins of the AIB were characterized by two different sedimentary successions (stratigraphic units-1 and -2 in Figure 2). In particular, the upper Calabrian palustrine deposits of the Madonna della Strada Fm. are only present in the ASB sedimentary succession and are absent within the PSC. Additionally, the upper Piacenzian-lower Calabrian lacustrine facies (San Nicandro Fm.) are exclusively present within the PSC and abruptly terminate, to the west, in correspondence with the basin-boundary fault (Bazzano-Fossa Fault, BFF), as depicted in the geological cross sections by Nocentini et al. (2018) (Figure 12a). This scenario is also highlighted by high-resolution seismic imaging that indicates the

10.1029/2024TC008548

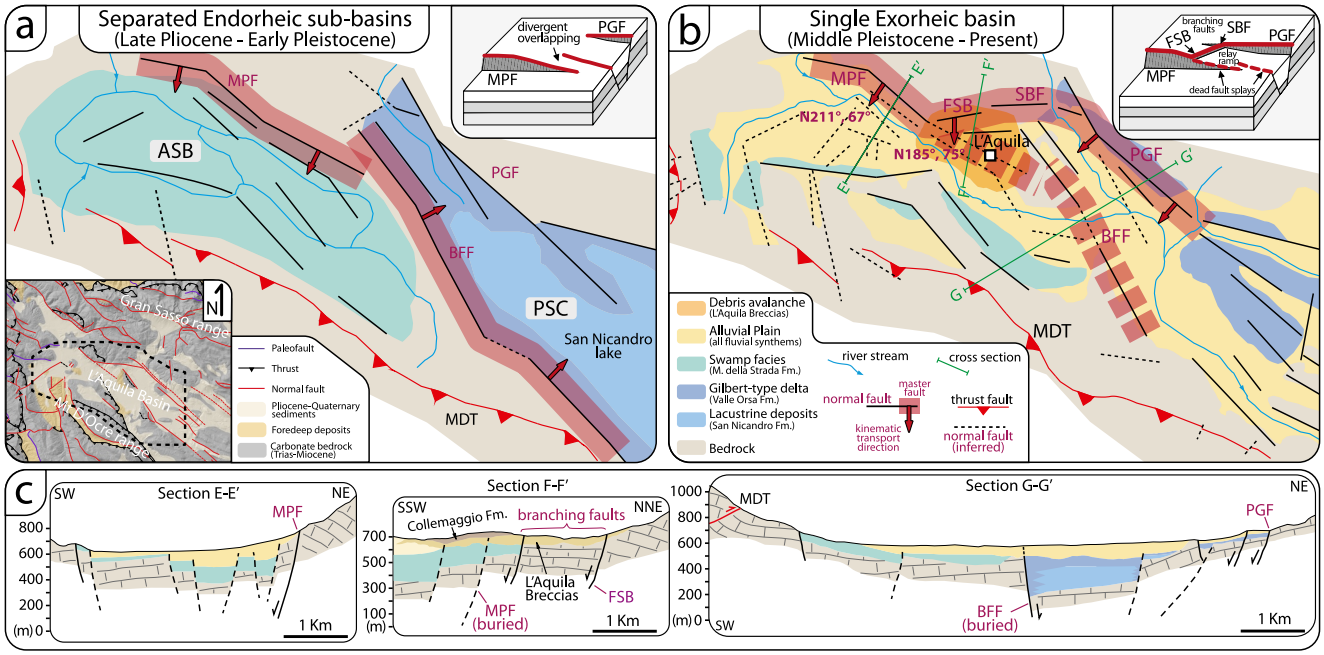

Figure 12. Schematic evolution of the L'Aquila Intermontane Basin (AIB) during the Late Pliocene-Quaternary. (a) During the late Piacenzian-early Calabrian (Late Pliocene—Early Pleistocene) ASB and PSC were experiencing distinct tectono-stratigraphic evolutions, with sediment deposition controlled by internally drained conditions, (separated endorheic sub-basins). The two sub-basins were structurally separated by the Bazzano-Fossa normal fault (BFF), which generated a topographic relief that acted as a structural barrier (watershed). (b) Since the Late-Middle Pleistocene AIB evolved to a distributed fluvial-alluvial plain by river catchment that transitioned the separated sub-basins to a single externally drained basin (exorheic). This transition is accompanied by a strong decrease in the tectonic activity of the BFF occurred at least since 0.8–0.6 Myr. Such transition is likely linked to the development of a transfer zone between the MPF and the PGF-SBF, which shifted the localization of the slip along the main faults, forcing the decrease in activity in the BFF. (c) Simplified geological cross sections highlighting the stratigraphical differences between ASB and PSC and the role of the BFF in separating the sub-basins until they get sealed by the Aterno Valley fluvial plain deposits (section C-C′). ASB: L'Aquila-Scoppito Sub-basin; PSC: Paganica-San Demetrio-Castelnuovo Sub-basin; MPF: Mount Pettino Fault. FSB: Faults in L'Aquila Breccias Fm. (transfer zone). SBF: San Biagio Fault. PGF: Paganica Fault. BFF: Bazzano-Fossa Fault. MDT: Monti D'Ocre Thrust.

presence of a Late Pliocene sedimentary basin structurally controlled by the BFF (Bruno et al., 2022). These observations suggest the persistence of two endorheic sub-basins with limited surface connection from ~3 to 1.1 Ma, as constrained by the age of the San Nicandro paleolake deposits (Cosentino et al., 2017; Geurts et al., 2020; Nocentini et al., 2018; Spadi et al., 2016). It is inferred that, during that period, the BFF represented the structural barrier, as its footwall acted as a watershed between the ASB and PSC (Figure 12a).

Presently, such a structural barrier does not exist anymore, as the BFF and its footwall are incised by the Aterno River in correspondence of the Bazzano-Monticchio window (Figure 3). This is also evidenced by the continuous distribution of the Unit-3 sediments throughout the entire AIB. This indicates that the rate of river incision exceeded fault activity, which may have been caused by both an increase in climate related events (Geurts et al., 2018) and a decrease in tectonic activity. Indeed, over the past 0.8–0.6 Myr (at least), the BFF has exhibited a long-term slip rate that is significantly lower (0.02 and 0.05 mm/yr, see Section 5.2) than that of the adjacent basin boundary faults (MPF and Paganica Fault). This evidence suggests that the BBF did not play an active role in the tectono-stratigraphic evolution of the AIB during the last 0.8 Myr (at least), in contrast to what occurred during the Late Pliocene-Early Pleistocene (e.g., Bruno et al., 2022; Nocentini et al., 2017). Furthermore, a decrease in tectonic activity is also observed in the southeastern branch of the MPF since (at least) 0.3 Ma, being then sealed by the Collemaggio Upper Pleistocene (MIS 5e, ~125 ka) deposits (see Section 5.1). It is proposed that the deactivation of the BFF and the southeastern portion of the MPF during the Late Pleistocene, were caused by the progressive slip localization along the antithetic Paganica fault system and its connection with the SBF and the MPF. This scenario is corroborated by the tectonic activity observed in the overlay zone between the MPF and the PGF-SBF, which occurred at least from 0.33 to 0.18 Ma, with slip rates comparable to those of the MPF (~0.2–0.3 mm/yr). It is possible that this hard linkage may have induced the quasi-abandonment of both the BFF fault and the

southeastern portion of the MPF (dead fault splays; Figure 12b), as evidenced by the decrease in the estimated long-term slip rates, which consequently suggest a reduction in their activity (Section 5.2).

Between 1.2 and 1.1 Ma (age of the latest lacustrine deposits of Unit-1) and 0.8–0.6 Ma (age of the oldest fluvial deposits of the Unit-3), the endorheic conditions of the AIB transitioned to exorheic drainage by the development of distributed fluvial connections related to the Aterno River system (Geurts et al., 2020). We advocate that the propagation of faulting at the junction between the sub-basins, combined with increasing sediment and water supply in the area during the Pleistocene (Geurts et al., 2018, 2020) promoted the transition from separated endorheic sub-basins to the formation of a continuous alluvial plain through the entire AIB (Figure 12b). This interplay promoted the development of drainage-parallel structures at the expense of drainage-orthogonal faults (BFF), which appear incised by the river network. Based on the available data and the results of this work, we infer that the structural connection of the MPF and PGF fault system occurred within the time frame of 1.1–0.8 Ma and continued its activity, at least, at 0.33–0.18 Ma.

5.3.1. The Volcaniclastic Deposit of San Giuliano Convent

Tephra layers and volcanic deposits are commonly found in the sedimentary sequences of the central Apennine Intermontane basins, such as the Fucino, L'Aquila, and Sulmona basins (Figure S2 in Supporting Information S1) (Giaccio et al., 2013; Monaco et al., 2021). These deposits originate from the Tyrrhenian margin of the Italian Peninsula, which was characterized by HK-calcalkaline to K-alkaline volcanisms that was active from the Middle to the Late Pleistocene (Peccerillo, 2005). Dating tephra layers in tectonic-sedimentary successions contributes to the development of age models for continental sedimentary systems, which provides constraints on the activity of the sedimentary basin boundary faults. We documented the presence of a volcaniclastic deposit located at Sampling Site-3. The $^{40}Ar/^{39}Ar$ age is 416.88 ± 0.70 ka (Figure 9; data in Data Set S1), which falls within the age of the Tufi Stratificati Varicolori di La Storta (Mattias & Ventriglia, 1970), dated 416 ± 6 ka by Karner et al. (2001). This deposit corresponds to a succession composed of alternating piroclastites, fallout pumices and reworked volcaniclastic levels from the Sabatini Volcanic Complex, northward of the city of Rome (Figure S2 in Supporting Information S1). It is proposed that the fall products of this huge volcanic eruption arrived into the L'Aquila Basin, allowing the formation of the S. Giuliano Convent outcrop. However, despite the similarity both in age and the bulk composition with the Tufi Stratificati Varicolori di La Storta, the correct attribution of this volcaniclastic deposit should be addressed with petrographic and chemical investigations, which are beyond the scope of the work.

5.4. Seismotectonic Implications

The definition of active faults in seismic hazard assessments is a complex task that requires targeted multidisciplinary analyses and a thorough understanding of the local seismotectonic regime. In the central Apennines, a fault is generally deemed potentially active if it exhibits evidence of activity within the past 40 kyr (Galadini et al., 2012, and references therein). Long-term tectono-stratigraphic studies may contribute to refine the present-day seismotectonic behavior of an active fault. When analyzing the surface ruptures during the 2009 L'Aquila earthquake, it appears mostly confined along the Paganica fault system, propagating toward the north, with very few co-seismic ruptures in the MPF area (Boncio et al., 2010; Falcucci et al., 2009). From a structural point of view, this tectonic "bypass" might suggest that the two faults are not structurally linked. Nevertheless, our findings highlighted the occurrence of tectonic activity along the MPF during the late Middle Pleistocene (0.33–0.18 Ma), with hard-linkage faulting in the overlay zone between the MPF and the PGF-SBF fault system. This geological evidence attests to a structural connection between the Upper and Middle segments of the Aterno Valley fault system. Such a tectonic connection has been hypothesized by several authors to resolve historical seismicity (Boncio et al., 2004; Galli et al., 2010, 2011) and seismological data (Falcucci et al., 2015), as the Aterno Valley fault segments are thought to have been simultaneously activated to generate >Mw 6.5 earthquakes (Vittori et al., 2011); for example, the 1703 Mw 6.7 earthquake; (Figure 1d). Moreover, numerical modeling on branched normal fault segments shows that, even with modest interaction within the fault segments at the surface, a fault rupture can break the entire fault length at depth, producing larger earthquake ruptures than what it is expected from the surface length of the single segment (Soliva et al., 2008). Although our results did not provide any evidence of historical (<40 kyr) activation of the transfer faults in the MPF overlay zone, our geological data are relevant to support the hypothesis that the eastern margin of the L'Aquila Basin is structurally connected at the surface.

5.5. Geodynamic Insights

In the central Apennines, deep geodynamic processes coexist with tectonic and geomorphological processes in shaping the surface. Throughout the Quaternary, the predominant geodynamic forcing in the central Apennines has been the upward movement of the mantle (Cosentino et al., 2017; D'Agostino et al., 2001; Faccenna, Becker, Miller, et al., 2014; Lanari et al., 2023; San Jose et al., 2020). Several authors suggest that the regional Late Pliocene–Quaternary uplift is related to a transition from Adriatic slab roll-back to slab break-off (Cosentino et al., 2017; Fellin et al., 2021; Lanari et al., 2023; Racano et al., 2024). This process significantly influences both the evolution of the landscape and the pattern of ongoing deformations in the region (D'Agostino et al., 2001). This hypothesis is supported by the symmetry in the topographic bulge and the drainage divide (D'Agostino et al., 2001; Lanari et al., 2023), by geomorphological evidence (e.g., Galadini et al., 2003), and by the synchronous occurrence of the regional uplift and the syn rift deposits during the Late Pliocene (Cosentino et al., 2017). In Section 5.1 it is inferred that the amount of exhumation of the MPF fault core is almost exclusively related to tectonic processes. Noteworthy, this amount of the tectonically driven exhumation (1.4–2.1 km) is in the order of magnitude of the amount of surface uplift registered by the Late Pliocene- Quaternary rocks in the central Apennines, which has been estimated at ∼1.3–2 km (Racano et al., 2024; San Jose et al., 2020). Given that the two processes are coeval, it may be inferred that the long-term rates of tectonic exhumation of the MPF and uplift on the central Apennines are comparable, with a range of 0.4–0.7 km/Ma. This inference supports the hypothesis that the geodynamic engine (Adriatic slab break-off) has been exerting a direct influence on the long-term morphotectonic evolution of the central Apennines since the Late Pliocene.

6. Conclusion

The main results from this study are:

- The tectono-stratigraphic evolution along the eastern boundary fault of the AIB is characterized by a polyphase tectonic history, recording transition from localized to delocalized deformation and fault linkage along the Mount Pettino Fault (MPF) and the adjacent Paganica (PGF) and San Biagio (SBF) faults.
- The early stage (Stage-1 faulting) is documented by the exhumed fault core of the MPF, which developed in a closed geochemical system in equilibrium with the circulating fluids at T ranging between 33 and 50°C (derived from Δ_{47}).
- The overlay zone between the MPF and the PGF-SBF faults consists of a branching fault system that served as the structural connection between the basin boundary faults of the L'Aquila Basin (Stage-2 faulting). This fault activity is associated with syn-tectonic carbonate structures developed in an open system, with fluids at T around 7–8°C (Δ_{47}). Geochronological constraints place this structural connection at least in the 331–182 ka time frame.
- The hard linkage between the MPF and the PGF-SBF might be the evidence for a long-lived (from ∼1 to ∼0.3 Ma) fault interaction and linkage that favored the transition from separated endorheic sub-basins to a single interconnected exorheic basin. The identified structural connection has relevant implications for refining the seismotectonic scenario of central Italy.
- The MPF fault core was tectonically exhumed from depths of ∼1.4–2.1 km since the Late Pliocene. The amount of tectonically driven exhumation of the MPF and the magnitude of regional uplift of the central Apennines are almost identical, supporting the hypothesis that deeply rooted inference has been exerting primary control on the morphotectonic evolution of the region. Such influence can be directly investigated on exhumed tectonic structures.

This work emphasizes how understanding the long-term tectono-stratigraphic evolution of the Late Pliocene-Quaternary extensional intermontane basins of central Italy may help improve the seismotectonic, morphotectonic and geodynamic scenario of the region.

Data Availability Statement

We provide online supplementary material in the Supporting Information files. File S1 contains the analytical protocols and detailed methodological procedures as well as additional results and figures. Data Sets S1 and S2 contain the results of the Ar-Ar and clumped isotopes analyses, respectively. All the data and results supporting

the findings of this article are also stored and available for download from Mendeley Data (https://data.mendeley.com/datasets/zn6trh96zw/5) (Arriga et al., 2024 [Dataset]).

Acknowledgments
Ph C thanks the Research Foundation Flanders project (G038022N) & Hercules program for instrument funding and the VUB Strategic Program for lab support. U-Th dating was supported by grants from the National Science and Technology Council, Taiwan, ROC (111-2116-M-002-022 to C.-C.S.), the Higher Education Sprout Project of the Ministry of Education, Taiwan ROC (112L901001 to C.-C.S.), the National Taiwan University (112L894202 to C.-C.S.). The authors thank Prof. David Phillips and Stan Szczepanski for assistance with the Ar-Ar analyses at the AuScope supported Noble Gas Geochronology Laboratory at The University of Melbourne. GA, FR, and DC thank the funds granted to the Department of Science (University of Roma Tre) through the 2018–2022 and 2023–2027 projects of excellence (Dipartimento di Eccellenza) by MUR-Italy. Special thanks to Prof. Francesco Salvini for the useful discussions on the structural analyses. The authors thank three anonymous reviewers of the early submitted version, whose comments helped to improve the clarity and quality of the manuscript.

References

Acocella, F., Funiciello, Rossetti, & Rossetti (1999). Sand-box modelling of basement-controlled transfer zones in extensional domains. *Terra Nova*, *11*(4), 149–156. https://doi.org/10.1046/j.1365-3121.1999.00238.x

Agostini, S., Palombo, M. R., Rossi, M. A., Di Canzio, E., & Tallini, M. (2012). Mammuthus meridionalis (Nesti, 1825) from Campo di Pile (L'Aquila, Abruzzo, central Italy). *Quaternary International*, *276–277*, 42–52. https://doi.org/10.1016/j.quaint.2012.05.013

Amoroso, S., Del Monaco, F., Di Eusebio, F., Monaco, P., Taddei, B., Tallini, M., et al. (2010). Campagna di indagini geologiche, geotecniche e geofisiche per lo studio della risposta sismica locale della città dell'Aquila: La stratigrafia dei sondaggi giugno-agosto 2010. *CERFIS-Centro Di Ricerca e Formazione in Ingegneria Sismica, Università Dell'Aquila, Pubblicazione CERFIS*, *1*(10).

Anderson, N. T., Kelson, J. R., Kele, S., Daëron, M., Bonifacie, M., Horita, J., et al. (2021). A unified clumped isotope thermometer calibration (0.5–1,100°C) using carbonate-based standardization. *Geophysical Research Letters*, *48*(7), e2020GL092069. https://doi.org/10.1029/2020GL092069

Antonielli, B., Della Seta, M., Esposito, C., Scarascia Mugnozza, G., Schilirò, L., Spadi, M., & Tallini, M. (2020). Quaternary rock avalanches in the Apennines: New data and interpretation of the huge clastic deposit of the L'Aquila Basin (central Italy). *Geomorphology*, *361*, 107194. https://doi.org/10.1016/j.geomorph.2020.107194

Arriga, G., Marchegiano, M., Peral, M., Hu, H.-M., Cosentino, D., Shen, C.-C., et al. (2024). Long-term tectono-stratigraphic evolution of a propagating rift system, L'Aquila Intermountain Basin (central Apennines) [Dataset]. *Mendeley Data, V5*. https://doi.org/10.17632/zn6trh96zw.5

Bally, A. W. (1986). Balanced sections and seismic reflection profiles across the central Apennines. *Memeorie della Società Geologica Italiana*, *35*, 257–310.

Bassi, G. (1991). Factors controlling the style of continental rifting: Insights from numerical modelling. *Earth and Planetary Science Letters*, *105*(4), 430–452. https://doi.org/10.1016/0012-821X(91)90183-I

Bertini, T., & Bosi, C. (1993). La tettonica quaternaria della conca di Fossa (L'Aquila). *Il Quaternario*, *6*(2), 293–314.

Bigi, G., Cosentino, D., Parotto, M., Sartori, R., & Scandone, P. (1992). Structural model of Italy 1: 500,000. *CNR Progetto Finalizzato Geodinamica*, *114*(3).

Blumetti, A. M., & Guerrieri, L. (2007). Fault-generated mountain fronts and the identification of fault segments: Implications for seismic hazard assessment. *Bollettino della Societa Geologica Italiana*, *126*(2), 307.

Boncio, P., Lavecchia, G., & Pace, B. (2004). Defining a model of 3D seismogenic sources for seismic hazard assessment applications: The case of central Apennines (Italy). *Journal of Seismology*, *8*(3), 407–425. https://doi.org/10.1023/B:JOSE.0000038449.78801.05

Boncio, P., Pizzi, A., Brozzetti, F., Pomposo, G., Lavecchia, G., Di Naccio, D., & Ferrarini, F. (2010). Coseismic ground deformation of the 6 April 2009 L'Aquila earthquake (central Italy, Mw6.3). *Geophysical Research Letters*, *37*(6), L06308. https://doi.org/10.1029/2010GL042807

Bosi, C., & Messina, P. (1991). Ipotesi di correlazione fra successioni morfo-litostratigrafiche plio-pleistoceniche nell'Appennino Laziale-Abruzzese. *Studi Geologici Camerti*, *2*, 257–263.

Brogi, A., Alçiçek, M. C., Liotta, D., Capezzuoli, E., Zucchi, M., & Matera, P. F. (2021). Step-over fault zones controlling geothermal fluid-flow and travertine formation (Denizli Basin, Turkey). *Geothermics*, *89*, 101941. https://doi.org/10.1016/j.geothermics.2020.101941

Bruno, P. P. G., Villani, F., & Improta, L. (2022). High-resolution seismic imaging of fault-controlled basins: A case study from the 2009 Mw 6.1 central Italy earthquake. *Tectonics*, *41*(4), e2022TC007207. https://doi.org/10.1029/2022TC007207

Brunori, C. A., Civico, R., Cinti, F. R., & Ventura, G. (2013). Characterization of active fault scarps from LiDAR data: A case study from central Apennines (Italy). *International Journal of Geographical Information Science*, *27*(7), 1405–1416. https://doi.org/10.1080/13658816.2012.684385

Buck, W. R. (1991). Modes of continental lithospheric extension. *Journal of Geophysical Research*, *96*(B12), 20161–20178. https://doi.org/10.1029/91JB01485

Butler, R. W. H., Mazzoli, S., Corrado, S., Donatis, M. D., Bucci, D. D., Gambini, R., et al. (2004). Applying thick-skinned tectonic models to the Apennine thrust belt of Italy—Limitations and implications. In *Thrust tectonics and hydrocarbon systems*. American Association of Petroleum Geologists. https://doi.org/10.1306/M82813C34

Carannante, S., Monachesi, G., Cattaneo, M., Amato, A., & Chiarabba, C. (2013). Deep structure and tectonics of the northern-central Apennines as seen by regional-scale tomography and 3-D located earthquakes. *Journal of Geophysical Research: Solid Earth*, *118*(10), 5391–5403. https://doi.org/10.1002/jgrb.50371

Carboni, F., Brozzetti, F., Mirabella, F., Cruciani, F., Porreca, M., Ercoli, M., et al. (2020). Geological and geophysical study of a thin-skinned tectonic wedge formed during an early collisional stage: The trasimeno tectonic wedge (Northern Apennines, Italy). *Geological Magazine*, *157*(2), 213–232. https://doi.org/10.1017/S001675681900061X

Carminati, E., & Doglioni, C. (2012). Alps vs. Apennines: The paradigm of a tectonically asymmetric Earth. *Earth-Science Reviews*, *112*(1), 67–96. https://doi.org/10.1016/j.earscirev.2012.02.004

Cartwright, J. A., Trudgill, B. D., & Mansfield, C. S. (1995). Fault growth by segment linkage: An explanation for scatter in maximum displacement and trace length data from the Canyonlands Grabens of SE Utah. *Journal of Structural Geology*, *17*(9), 1319–1326. https://doi.org/10.1016/0191-8141(95)00033-A

Cavinato, G. P., & Celles, P. G. D. (1999). Extensional basins in the tectonically bimodal central Apennines fold-thrust belt, Italy: Response to corner flow above a subducting slab in retrograde motion. *Geology*, *27*(10), 955–958. https://doi.org/10.1130/0091-7613(1999)027<0955:EBITTB>2.3.CO;2

Cavinato, G. P., Cosentino, D., De Rita, D., Funiciello, R., & Parotto, M. (1994). Tectonic-sedimentary evolution of intrapenninic basins and correlation with the volcano-tectonic activity in central Italy. *Memorie Descrittive della Carta Geologica d'Italia*, *49*, 63–76.

Cavinato, G. P., Salvini, F., & Tozzi, M. (1986). Evoluzione tettonica del settore centrale della linea Olevano-Antrodoco: Il contributo dell'analisi strutturale. *Geologia Dell'Italia Centrale. Congresso Nazionale.*, *73*, 225–228.

Centamore, E., Crescenti, U., & Dramis, F. (2006). *Note illustrative della Carta Geologica d'Italia alla scala 1:50.000, Foglio 359-L'Aquila* (p. 128). APAT-Dipartimento Difesa Del Suolo-Servizio Geologico d'Italia, Ente Realizzatore Regione Abruzzo. Retrieved from http://www.isprambiente.gov.it/Media/carg/note_illustrative/359_LAquila.pdf

Centamore, E., & Dramis, F. (2010). *Note illustrative della Carta Geologica d'Italia alla scala 1: 50.000, Foglio 358-Pescorocchiano* (p. 147). ISPRA-Servizio Geologico d'Italia, Ente Realizzatore Regione Lazio. Retrieved from http://www.isprambiente.gov.it/Media/carg/note_illustrative/358_Pescorocchiano.pdf

Centamore, E., & Rossi, D. (2009). Neogene-Quaternary tectonics and sedimentation in the central Apennines. *Italian Journal of Geosciences*, *128*(1), 73–88.

Cheloni, D., D'Agostino, N., D'Anastasio, E., Avallone, A., Mantenuto, S., Giuliani, R., et al. (2010). Coseismic and initial post-seismic slip of the 2009 Mw 6.3 L'Aquila earthquake, Italy, from GPS measurements. *Geophysical Journal International*, *181*(3), 1539–1546. https://doi.org/10.1111/j.1365-246X.2010.04584.x

Cheng, H., Lawrence Edwards, R., Shen, C.-C., Polyak, V. J., Asmerom, Y., Woodhead, J., et al. (2013). Improvements in ^{230}Th dating, ^{230}Th and ^{234}U half-life values, and U–Th isotopic measurements by multi-collector inductively coupled plasma mass spectrometry. *Earth and Planetary Science Letters*, *371–372*, 82–91. https://doi.org/10.1016/j.epsl.2013.04.006

Chiaraluce, L., Valoroso, L., Piccinini, D., Di Stefano, R., & De Gori, P. (2011). The anatomy of the 2009 L'Aquila normal fault system (central Italy) imaged by high resolution foreshock and aftershock locations. *Journal of Geophysical Research*, *116*(B12), B12311. https://doi.org/10.1029/2011JB008352

Childs, C., Watterson, J., & Walsh, J. J. (1995). Fault overlap zones within developing normal fault systems. *Journal of the Geological Society*, *152*(3), 535–549. https://doi.org/10.1144/gsjgs.152.3.0535

Cipollari, P., & Cosentino, D. (1995). Miocene unconformities in the central Apennines: Geodynamic significance and sedimentary basin evolution. *Tectonophysics*, *252*(1), 375–389. https://doi.org/10.1016/0040-1951(95)00088-7

Cipollari, P., & Cosentino, D. (1996). Miocene tectono-sedimentary events and geodynamic evolution of the central Apennines (Italy). *Notes et Mémoires du Service géologique du Maroc*, *387*, 163–176.

Cipollari, P., Cosentino, D., Esu, D., Girotti, O., Gliozzi, E., & Praturlon, A. (1999). Thrust-top lacustrine–lagoonal basin development in accretionary wedges: Late Messinian (Lago-Mare) episode in the central Apennines (Italy). *Palaeogeography, Palaeoclimatology, Palaeoecology*, *151*(1), 149–166. https://doi.org/10.1016/S0031-0182(99)00026-7

Cipollari, P., Cosentino, D., & Gliozzi, E. (1999). Extension-and compression-related basins in central Italy during the Messinian Lago-Mare event. *Tectonophysics*, *315*(1–4), 163–185. https://doi.org/10.1016/s0040-1951(99)00287-5

Civico, R., Sapia, V., Di Giulio, G., Villani, F., Pucci, S., Baccheschi, P., et al. (2017). Geometry and evolution of a fault-controlled Quaternary basin by means of TDEM and single-station ambient vibration surveys: The example of the 2009 L'Aquila earthquake area, central Italy. *Journal of Geophysical Research: Solid Earth*, *122*(3), 2236–2259. https://doi.org/10.1002/2016JB013451

Cosentino, D., Asti, R., Nocentini, M., Gliozzi, E., Kotsakis, T., Mattei, M., et al. (2017). New insights into the onset and evolution of the central Apennine extensional intermontane basins based on the tectonically active L'Aquila Basin (central Italy). *GSA Bulletin*, *129*(9–10), 1314–1336. https://doi.org/10.1130/B31679.1

Cosentino, D., Cipollari, P., Marsili, P., & Scrocca, D. (2010). Geology of the central Apennines: A regional review. *Journal of the Virtual Explorer*, *36*(11), 1–37. https://doi.org/10.3809/jvirtex.2009.00223

Cowie, P. A., & Scholz, C. H. (1992). Growth of faults by accumulation of seismic slip. *Journal of Geophysical Research*, *97*(B7), 11085–11095. https://doi.org/10.1029/92JB00586

Crone, A. J., & Haller, K. M. (1991). Segmentation and the coseismic behavior of Basin and Range normal faults: Examples from east-central Idaho and southwestern Montana, U.S.A. *Journal of Structural Geology*, *13*(2), 151–164. https://doi.org/10.1016/0191-8141(91)90063-O

Curzi, M., Aldega, L., Bernasconi, S. M., Berra, F., Billi, A., Boschi, C., et al. (2020). Architecture and evolution of an extensionally-inverted thrust (Mt. Tancia Thrust, central Apennines): Geological, structural, geochemical, and K–Ar geochronological constraints. *Journal of Structural Geology*, *136*, 104059. https://doi.org/10.1016/j.jsg.2020.104059

Curzi, M., Aldega, L., Billi, A., Boschi, C., Carminati, E., Vignaroli, G., et al. (2024). Fossilchemical-physical (dis) equilibria between paleofluids and host rocks and their relationship to the seismiccycle and earthquakes. *Earth-Science Reviews*, *254*, 104801. https://doi.org/10.1016/j.earscirev.2024.104801

Curzi, M., Cipriani, A., Aldega, L., Billi, A., Carminati, E., der Lelij, R., et al. (2024). Architecture and permeability structure of the Sibillini Mts. Thrust and influence upon recent, extension-related seismicity in the central Apennines (Italy) through fault-valve behavior. *GSA Bulletin*, *136*(1–2), 3–26. https://doi.org/10.1130/B36616.1

D'Agostino, N., Cheloni, D., Fornaro, G., Giuliani, R., & Reale, D. (2012). Space-time distribution of afterslip following the 2009 L'Aquila earthquake. *Journal of Geophysical Research*, *117*(B2), B02402. https://doi.org/10.1029/2011JB008523

D'Agostino, N., Jackson, J. A., Dramis, F., & Funiciello, R. (2001). Interactions between mantle upwelling, drainage evolution and active normal faulting: An example from the central Apennines (Italy). *Geophysical Journal International*, *147*(2), 475–497. https://doi.org/10.1046/j.1365-246X.2001.00539.x

De Paola, N., Holdsworth, R. E., Collettini, C., Mccaffrey, K. J. W., & Barchi, M. R. (2007). The structural evolution of dilational stepovers in regional transtensional zones. *Geological Society, London, Special Publications*, *290*(1), 433–445. https://doi.org/10.1144/SP190.17

Dewey, J. F. (1988). Extensional collapse of orogens. *Tectonics*, *7*(6), 1123–1139. https://doi.org/10.1029/TC007i006p01123

Diaferia, G., Cammarano, F., & Faccenna, C. (2019). Thermal structure of a vanishing subduction system: An example of seismically-derived crustal temperature along the Italian peninsula. *Geophysical Journal International*, *219*(1), 239–247. https://doi.org/10.1093/gji/ggz289

Di Luccio, F., Ventura, G., Di Giovambattista, R., Piscini, A., & Cinti, F. R. (2010). Normal faults and thrusts reactivated by deep fluids: The 6 April 2009 Mw 6.3 L'Aquila earthquake, central Italy. *Journal of Geophysical Research*, *115*(B6), B06315. https://doi.org/10.1029/2009JB007190

Di Stefano, R., Chiarabba, C., Chiaraluce, L., Cocco, M., De Gori, P., Piccinini, D., & Valoroso, L. (2011). Fault zone properties affecting the rupture evolution of the 2009 (Mw 6.1) L'Aquila earthquake (central Italy): Insights from seismic tomography. *Geophysical Research Letters*, *38*(10), L10310. https://doi.org/10.1029/2011GL047365

Duffy, O. B., Bell, R. E., Jackson, C. A.-L., Gawthorpe, R. L., & Whipp, P. S. (2015). Fault growth and interactions in a multiphase rift fault network: Horda Platform, Norwegian North Sea. *Journal of Structural Geology*, *80*, 99–119. https://doi.org/10.1016/j.jsg.2015.08.015

Ebinger, C. (2005). Continental break-up: The East African perspective. *Astronomy and Geophysics*, *46*(2), 2.16–2.21. https://doi.org/10.1111/j.1468-4004.2005.46216.x

Eiler, J. M. (2011). Paleoclimate reconstruction using carbonate clumped isotope thermometry. *Quaternary Science Reviews*, *30*(25), 3575–3588. https://doi.org/10.1016/j.quascirev.2011.09.001

Elter, F. M., Elter, P., Eva, C., Eva, E., Kraus, R. K., Padovano, M., & Solarino, S. (2012). An alternative model for the recent evolution of the northern–central Apennines (Italy). *Journal of Geodynamics*, *54*, 55–63. https://doi.org/10.1016/j.jog.2011.11.001

Elter, P., Grasso, M., Parotto, M., & Vezzani, L. (2003). Structural setting of the Apennine-Maghrebian thrust belt. *Episodes Journal of International Geoscience*, *26*(3), 205–211. https://doi.org/10.18814/epiiugs/2003/v26i3/009

Endignoux, L., Moretti, I., & Roure, F. (1989). Forward modeling of the southern Apennines. *Tectonics*, *8*(5), 1095–1104. https://doi.org/10.1029/tc008i005p01095

Faccenna, C., Becker, T. W., Auer, L., Billi, A., Boschi, L., Brun, J. P., et al. (2014). Mantle dynamics in the Mediterranean. *Reviews of Geophysics*, *52*(3), 283–332. https://doi.org/10.1002/2013RG000444

Faccenna, C., Becker, T. W., Lucente, F. P., Jolivet, L., & Rossetti, F. (2001). History of subduction and back arc extension in the central Mediterranean. *Geophysical Journal International*, *145*(3), 809–820. https://doi.org/10.1046/j.0956-540x.2001.01435.x

Faccenna, C., Becker, T. W., Miller, M. S., Serpelloni, E., & Willett, S. D. (2014). Isostasy, dynamic topography, and the elevation of the Apennines of Italy. *Earth and Planetary Science Letters*, *407*, 163–174. https://doi.org/10.1016/j.epsl.2014.09.027

Faccenna, C., Mattei, M., Funiciello, R., & Jolivet, L. (1997). Styles of back-arc extension in the central Mediterranean. *Terra Nova*, *9*(3), 126–130. https://doi.org/10.1046/j.1365-3121.1997.d01-12.x

Falcone, R. A., Falgiani, A., Parisse, B., Petitta, M., Spizzico, M., & Tallini, M. (2008). Chemical and isotopic ($\delta^{18}O‰$, $\delta^{2}H‰$, $\delta^{13}C‰$, ^{222}Rn) multi-tracing for groundwater conceptual model of carbonate aquifer (Gran Sasso INFN underground laboratory—Central Italy). *Journal of Hydrology*, *357*(3), 368–388. https://doi.org/10.1016/j.jhydrol.2008.05.016

Falcucci, E., Gori, S., Moro, M., Fubelli, G., Saroli, M., Chiarabba, C., & Galadini, F. (2015). Deep reaching versus vertically restricted Quaternary normal faults: Implications on seismic potential assessment in tectonically active regions: Lessons from the middle Aterno valley fault system, central Italy. *Tectonophysics*, *651–652*, 186–198. https://doi.org/10.1016/j.tecto.2015.03.021

Falcucci, E., Gori, S., Peronace, E., Fubelli, G., Moro, M., Saroli, M., et al. (2009). The Paganica fault and surface coseismic ruptures caused by the 6 April 2009 earthquake (L'Aquila, central Italy). *Seismological Research Letters*, *80*(6), 940–950. https://doi.org/10.1785/gssrl.80.6.940

Fellin, M. G., Jose, M. S., Faccenna, C., Willett, S. D., Cosentino, D., Lanari, R., et al. (2021). Transition from slab roll-back to slab break-off in the central Apennines, Italy: Constraints from the stratigraphic and thermochronologic record. *GSA Bulletin*, *134*(7–8), 1916–1930. https://doi.org/10.1130/B36123.1

Ferraro, F., Grieco, D. S., Agosta, F., & Prosser, G. (2018). Space-time evolution of cataclasis in carbonate fault zones. *Journal of Structural Geology*, *110*, 45–64. https://doi.org/10.1016/j.jsg.2018.02.007

Fossen, H., & Rotevatn, A. (2016). Fault linkage and relay structures in extensional settings—A review. *Earth-Science Reviews*, *154*, 14–28. https://doi.org/10.1016/j.earscirev.2015.11.014

Galadini, F. (1999). Pleistocene changes in the central Apennine fault kinematics: A key to decipher active tectonics in central Italy. *Tectonics*, *18*(5), 877–894. https://doi.org/10.1029/1999TC900020

Galadini, F., Falcucci, E., Galli, P., Giaccio, B., Gori, S., Messina, P., et al. (2012). Time intervals to assess active and capable faults for engineering practices in Italy. *Engineering Geology*, *139–140*, 50–65. https://doi.org/10.1016/j.enggeo.2012.03.012

Galadini, F., & Galli, P. (2000). Active tectonics in the central Apennines (Italy)–input data for seismic hazard assessment. *Natural Hazards*, *22*(3), 225–268. https://doi.org/10.1023/A:1008149531980

Galadini, F., & Messina, P. (2004). Early–Middle Pleistocene eastward migration of the Abruzzi Apennine (central Italy) extensional domain. *Journal of Geodynamics*, *37*(1), 57–81. https://doi.org/10.1016/j.jog.2003.10.002

Galadini, F., Messina, P., Giaccio, B., & Sposato, A. (2003). Early uplift history of the Abruzzi Apennines (central Italy): Available geomorphological constraints. *Quaternary International*, *101–102*, 125–135. https://doi.org/10.1016/S1040-6182(02)00095-2

Galli, P., Galadini, F., & Pantosti, D. (2008). Twenty years of paleoseismology in Italy. *Earth-Science Reviews*, *88*(1), 89–117. https://doi.org/10.1016/j.earscirev.2008.01.001

Galli, P., Giaccio, B., & Messina, P. (2010). The 2009 central Italy earthquake seen through 0.5 Myr-long tectonic history of the L'Aquila faults system. *Quaternary Science Reviews*, *29*(27), 3768–3789. https://doi.org/10.1016/j.quascirev.2010.08.018

Galli, P., Giaccio, B., Messina, P., Peronace, E., & Zuppi, G. M. (2011). Palaeoseismology of the L'Aquila faults (central Italy, 2009, Mw 6.3 earthquake): Implications for active fault linkage. *Geophysical Journal International*, *187*(3), 1119–1134. https://doi.org/10.1111/j.1365-246X.2011.05233.x

Gawthorpe, R. L., & Hurst, J. M. (1993). Transfer zones in extensional basins: Their structural style and influence on drainage development and stratigraphy. *Journal of the Geological Society*, *150*(6), 1137–1152. https://doi.org/10.1144/gsjgs.150.6.1137

Gawthorpe, R. L., & Leeder, M. R. (2000). Tectono-sedimentary evolution of active extensional basins. *Basin Research*, *12*(3-4), 195–218. https://doi.org/10.1111/j.1365-2117.2000.00121.x

GEMINA, G. N. (1963). Ligniti e Torbe dell'Italia Continentale.

Geurts, A. H., Cowie, P. A., Duclaux, G., Gawthorpe, R. L., Huismans, R. S., Pedersen, V. K., & Wedmore, L. N. J. (2018). Drainage integration and sediment dispersal in active continental rifts: A numerical modelling study of the central Italian Apennines. *Basin Research*, *30*(5), 965–989. https://doi.org/10.1111/bre.12289

Geurts, A. H., Whittaker, A. C., Gawthorpe, R. L., & Cowie, P. A. (2020). Transient landscape and stratigraphic responses to drainage integration in the actively extending central Italian Apennines. *Geomorphology*, *353*, 107013. https://doi.org/10.1016/j.geomorph.2019.107013

Ghisetti, F., Kirschner, D. L., Vezzani, L., & Agosta, F. (2001). Stable isotope evidence for contrasting paleofluid circulation in thrust faults and normal faults of the central Apennines, Italy. *Journal of Geophysical Research*, *106*(B5), 8811–8825. https://doi.org/10.1029/2000jb900377

Ghisetti, F., & Vezzani, L. (1991). Thrust belt development in the central Apennines (Italy): Northward polarity of thrusting and out-of-sequence deformations in the Gran Sasso Chain. *Tectonics*, *10*(5), 904–919. https://doi.org/10.1029/91TC00902

Giaccio, B., Arienzo, I., Sottili, G., Castorina, F., Gaeta, M., Nomade, S., et al. (2013). Isotopic (Sr–Nd) and major element fingerprinting of distal tephras: An application to the Middle-Late Pleistocene markers from the Colli Albani volcano, central Italy. *Quaternary Science Reviews*, *67*, 190–206. https://doi.org/10.1016/j.quascirev.2013.01.028

Giaccio, B., Galli, P., Messina, P., Peronace, E., Scardia, G., Sottili, G., et al. (2012). Fault and basin depocentre migration over the last 2 Ma in the L'Aquila 2009 earthquake region, central Italian Apennines. *Quaternary Science Reviews*, *56*, 69–88. https://doi.org/10.1016/j.quascirev.2012.08.016

Giardini, D., Jiménez, M.-J., & Grünthal, G. (2003). European-Mediterranean seismic hazard map. *Scale*, *1*, 5000000.

Gibbs, A. D. (1984). Structural evolution of extensional basin margins. *Journal of the Geological Society*, *141*(4), 609–620. https://doi.org/10.1144/gsjgs.141.4.0609

Gori, S., Falcucci, E., Atzori, S., Chini, M., Moro, M., Serpelloni, E., et al. (2012). Constraining primary surface rupture length along the Paganica fault (2009 L'Aquila earthquake) with geological and geodetic (DInSAR and GPS) data. *Italian Journal of Geosciences*, *131*(3), 359–372. https://doi.org/10.3301/IJG.2012.21

Guerrieri, L., Baer, G., Hamiel, Y., Amit, R., Blumetti, A. M., Comerci, V., et al. (2010). InSAR data as a field guide for mapping minor earthquake surface ruptures: Ground displacements along the Paganica Fault during the 6 April 2009 L'Aquila earthquake. *Journal of Geophysical Research*, *115*(B12), B12331. https://doi.org/10.1029/2010JB007579

Gupta, S., Cowie, P. A., Dawers, N. H., & Underhill, J. R. (1998). A mechanism to explain rift-basin subsidence and stratigraphic patterns through fault-array evolution. *Geology*, *26*(7), 595–598. https://doi.org/10.1130/0091-7613(1998)026<0595:AMTERB>2.3.CO;2

Hiess, J., Condon, D. J., McLean, N., & Noble, S. R. (2012). $^{238}U/^{235}U$ systematics in terrestrial uranium-bearing minerals. *Science*, *335*(6076), 1610–1614. https://doi.org/10.1126/science.1215507

Huntington, K. W., & Petersen, S. V. (2023). Frontiers of carbonate clumped isotope thermometry. *Annual Review of Earth and Planetary Sciences*, *51*(1), 611–641. https://doi.org/10.1146/annurev-earth-031621-085949

Hus, R., De Batist, M., Klerkx, J., & Matton, C. (2006). Fault linkage in continental rifts: Structure and evolution of a large relay ramp in Zavarotny; Lake Baikal (Russia). *Journal of Structural Geology*, *28*(7), 1338–1351. https://doi.org/10.1016/j.jsg.2006.03.031

Iezzi, F., Roberts, G., Walker, J. F., & Papanikolaou, I. (2019). Occurrence of partial and total coseismic ruptures of segmented normal fault systems: Insights from the central Apennines, Italy. *Journal of Structural Geology*, *126*, 83–99. https://doi.org/10.1016/j.jsg.2019.05.003

Improta, L., Villani, F., Bruno, P. P., Castiello, A., De Rosa, D., Varriale, F., et al. (2012). High-resolution controlled-source seismic tomography across the Middle Aterno basin in the epicentral area of the 2009, Mw 6.3, L'Aquila earthquake (central Apennines, Italy). *Italian Journal of Geosciences*, *131*(3), 373–388. https://doi.org/10.3301/IJG.2011.35

ISIDe, W. G. (2007). Italian seismological instrumental and parametric database (ISIDe). https://doi.org/10.13127/ISIDE

ITHACA, W. G. (2019). *ITHACA (ITaly HAzard from CApable faulting), A database of active capable faults of the Italian territory. Version December 2019*. ISPRA Geological Survey of Italy. Retrieved from http://Sgi2.Isprambiente.It/Ithacaweb/Mappatura.Aspx

Karner, D. B., Marra, F., & Renne, P. R. (2001). The history of the Monti Sabatini and Alban Hills volcanoes: Groundwork for assessing volcanic-tectonic hazards for Rome. *Journal of Volcanology and Geothermal Research*, *107*(1), 185–219. https://doi.org/10.1016/S0377-0273(00)00258-4

Kim, S.-T., & O'Neil, J. R. (1997). Equilibrium and nonequilibrium oxygen isotope effects in synthetic carbonates. *Geochimica et Cosmochimica Acta*, *61*(16), 3461–3475. https://doi.org/10.1016/S0016-7037(97)00169-5

Kim, Y.-S., & Sanderson, D. J. (2010). Inferred fluid flow through fault damage zones based on the observation of stalactites in carbonate caves. *Journal of Structural Geology*, *32*(9), 1305–1316. https://doi.org/10.1016/j.jsg.2009.04.017

Kirkwood, D., Savard, M. M., & Chi, G. (2001). Microstructural analysis and geochemical vein characterization of the Salinic event and Acadian Orogeny: Evaluation of the hydrocarbon reservoir potential in eastern Gaspé. *Bulletin of Canadian Petroleum Geology*, *49*(2), 262–281. https://doi.org/10.2113/49.2.262

Lanari, R., Faccenna, C., Benedetti, L., Sembroni, A., Bellier, O., Menichelli, I., et al. (2021). Formation and persistence of extensional internally drained basins: The case of the Fucino Basin (central Apennines, Italy). *Tectonics*, *40*(6), e2020TC006442. https://doi.org/10.1029/2020TC006442

Lanari, R., Reitano, R., Faccenna, C., Agostinetti, N. P., & Ballato, P. (2023). Surface and crustal response to deep subduction dynamics: Insights from the Apennines, Italy. *Tectonics*, *42*(3), e2022TC007461. https://doi.org/10.1029/2022TC007461

Larsen, P.-H. (1988). Relay structures in a Lower Permian basement-involved extension system, East Greenland. *Journal of Structural Geology*, *10*(1), 3–8. https://doi.org/10.1016/0191-8141(88)90122-8

Lavecchia, G., Ferrarini, F., Brozzetti, F., De Nardis, R., Boncio, P., & Chiaraluce, L. (2012). From surface geology to aftershock analysis: Constraints on the geometry of the L'Aquila 2009 seismogenic fault system. *Italian Journal of Geosciences*, *131*(3), 330–347. https://doi.org/10.3301/IJG.2012.24

Maccagno, A. M. (1962). *L'Elephas meridionalis Nesti di contrada Madonna della strada Scoppito (L'Aquila)*. Guglielmo Genovese.

Maccagno, A. M. (1965). Nuovi ritrovamenti di resti elefantini nel Villafranchiano della Conca aquilana. *Stabilimento tipografico Genovese*.

Magri, D., Di Rita, F., & Palombo, M. R. (2010). An Early Pleistocene interglacial record from an intermontane basin of central Italy (Scoppito, L'Aquila). *Quaternary International*, *225*(1), 106–113. https://doi.org/10.1016/j.quaint.2009.04.005

Mancini, M., Cavuoto, G., Pandolfi, L., Petronio, C., Salari, L., & Sardella, R. (2012). Coupling basin infill history and mammal biochronology in a Pleistocene intramontane basin: The case of western L'Aquila Basin (central Apennines, Italy). *Quaternary International*, *267*, 62–77. https://doi.org/10.1016/j.quaint.2011.03.020

Mattias, P. P., & Ventriglia, U. (1970). *La regione vulcanica dei Monti Sabatini e Cimini*. Arti Grafiche Pacini Mariotti.

Monaco, L., Palladino, D. M., Gaeta, M., Marra, F., Sottili, G., Leicher, N., et al. (2021). Mediterranean tephrostratigraphy and peri-Tyrrhenian explosive activity revaluated in light of the 430-365 ka record from Fucino Basin (central Italy). *Earth-Science Reviews*, *220*, 103706. https://doi.org/10.1016/j.earscirev.2021.103706

Mondati, G., Spadi, M., Gliozzi, E., Cosentino, D., Cifelli, F., Cavinato, G. P., et al. (2021). The tectono-stratigraphic evolution of the Fucino Basin (central Apennines, Italy): New insights from the geological mapping of its north-eastern margin. *Journal of Maps*, *17*(2), 87–100. https://doi.org/10.1080/17445647.2021.1880981

Mondy, L. S., Rey, P. F., Duclaux, G., & Moresi, L. (2017). The role of asthenospheric flow during rift propagation and breakup. *Geology*, *46*(2), 103–106. https://doi.org/10.1130/G39674.1

Morley, C. K., Nelson, R. A., Patton, T. L., & Munn, S. G. (1990). Transfer zones in the East African Rift System and their relevance to hydrocarbon exploration in rifts. *AAPG Bulletin*, *74*(8), 1234–1253. https://doi.org/10.1306/0C9B2475-1710-11D7-8645000102C1865D

Niespolo, E. M., Rutte, D., Deino, A. L., & Renne, P. R. (2017). Intercalibration and age of the Alder Creek sanidine $^{40}Ar/^{39}Ar$ standard. *Quaternary Geochronology*, *39*, 205–213. https://doi.org/10.1016/j.quageo.2016.09.004

Nocentini, M., Asti, R., Cosentino, D., Durante, F., Gliozzi, E., Macerola, L., & Tallini, M. (2017). Plio-Quaternary geology of L'Aquila—Scoppito Basin (central Italy). *Journal of Maps*, *13*(2), 563–574. https://doi.org/10.1080/17445647.2017.1340910

Nocentini, M., Cosentino, C., Spadi, M., & Tallini, M. (2018). Plio-Quaternary geology of the Paganica-San Demetrio-Castelnuovo Basin (central Italy). *Journal of Maps*, *14*(2), 411–420. https://doi.org/10.1080/17445647.2018.1481774

Nooitgedacht, C. W., van der Lubbe, H. J. L., de Graaf, S., Ziegler, M., Staudigel, P. T., & Reijmer, J. J. G. (2021). Restricted internal oxygen isotope exchange in calcite veins: Constraints from fluid inclusion and clumped isotope-derived temperatures. *Geochimica et Cosmochimica Acta*, *297*, 24–39. https://doi.org/10.1016/j.gca.2020.12.008

Olsen, K. H. (1995). *Continental rifts: Evolution, structure, tectonics*. Elsevier.

Parotto, M., & Praturlon, A. (1975). Geological summary of the central Apennines. *Quaderni de La Ricerca Scientifica*, *90*, 257–311.

Passey, B. H., & Henkes, G. A. (2012). Carbonate clumped isotope bond reordering and geospeedometry. *Earth and Planetary Science Letters*, *351–352*, 223–236. https://doi.org/10.1016/j.epsl.2012.07.021

Patacca, E., Sartori, R., & Scandone, P. (1990). Tyrrhenian basin and Apenninic arcs: Kinematic relations since late Tortonian times. *Memorie della Societa Geologica Italiana*, *45*, 425–451.

Patacca, E., Scandone, P., Di Luzio, E., Cavinato, G. P., & Parotto, M. (2008). Structural architecture of the central Apennines: Interpretation of the CROP 11 seismic profile from the Adriatic coast to the orographic divide. *Tectonics*, *27*(3). https://doi.org/10.1029/2005TC001917

Patacca, E., & Scandone, P. (1989). Post-Tortonian mountain building in the Apennines. The role of the passive sinking of a relic lithospheric slab. *Atti Dei Convegni Lincei*, *80*, 157–176.

Peacock, D. C. P., Knipe, R. J., & Sanderson, D. J. (2000). Glossary of normal faults. *Journal of Structural Geology*, *22*(3), 291–305. https://doi.org/10.1016/S0191-8141(00)80102-9

Peacock, D. C. P., & Sanderson, D. J. (1991). Displacements, segment linkage and relay ramps in normal fault zones. *Journal of Structural Geology*, *13*(6), 721–733. https://doi.org/10.1016/0191-8141(91)90033-F

Peccerillo, A. (2005). *Plio-quaternary volcanism in Italy* (Vol. 365). Springer.

Phillips, D., Matchan, E. L., Dalton, H., & Kuiper, K. F. (2022). Revised astronomically calibrated $^{40}Ar/^{39}Ar$ ages for the Fish Canyon Tuff sanidine—Closing the interlaboratory gap. *Chemical Geology*, *597*, 120815. https://doi.org/10.1016/j.chemgeo.2022.120815

Pizzi, A., Calamita, F., Coltorti, M., & Pieruccini, P. (2002). Quaternary normal faults, intramontane basins and seismicity in the Umbria-Marche-Abruzzi Apennine Ridge (Italy): Contribution of neotectonic analysis to seismic hazard assessment. *Bollettino della Società Geologica Italiana*, *1*, 923–929.

Powell, R., Green, E. C. R., Marillo Sialer, E., & Woodhead, J. (2020). Robust isochron calculation. *Geochronology*, *2*(2), 325–342. https://doi.org/10.5194/gchron-2-325-2020

Pucci, S., Villani, F., Civico, R., Di Naccio, D., Porreca, M., Benedetti, L., et al. (2019). Complexity of the 2009 L'Aquila earthquake causative fault system (Abruzzi Apennines, Italy) and effects on the Middle Aterno Quaternary basin arrangement. *Quaternary Science Reviews*, *213*, 30–66. https://doi.org/10.1016/j.quascirev.2019.04.014

Puliti, I., Pucci, S., Villani, F., Porreca, M., Benedetti, L., Robustelli, G., et al. (2022). Estimating the long-term slip rate of active normal faults: The case of the Paganica Fault (central Apennines, Italy). *Geomorphology*, *415*, 108411. https://doi.org/10.1016/j.geomorph.2022.108411

Racano, S., van der Beek, P. A., Schildgen, T. F., Faccenna, C., Buleo Tebar, V., & Cosentino, D. (2024). Slab driven Quaternary rock-uplift and topographic evolution in the northern-central Apennines from linear inversion of the drainage system. *Geochemistry, Geophysics, Geosystems*, *25*(7), e2024GC011592. https://doi.org/10.1029/2024GC011592

Reston, T. J., & Pérez-Gussinyé, M. (2007). Lithospheric extension from rifting to continental breakup at magma-poor margins: Rheology, serpentinisation and symmetry. *International Journal of Earth Sciences*, *96*(6), 1033–1046. https://doi.org/10.1007/s00531-006-0161-z

Ring, U., Brandon, M. T., Willett, S. D., & Lister, G. S. (1999). Exhumation processes. *Geological Society, London, Special Publications*, *154*(1), 1–27. https://doi.org/10.1144/gsl.sp.1999.154.01.01

Rivera, T. A., Storey, M., Schmitz, M. D., & Crowley, J. L. (2013). Age intercalibration of $^{40}Ar/^{39}Ar$ sanidine and chemically distinct U/Pb zircon populations from the Alder Creek Rhyolite Quaternary geochronology standard. *Chemical Geology*, *345*, 87–98. https://doi.org/10.1016/j.chemgeo.2013.02.021

Roberts, G. P., & Michetti, A. M. (2004). Spatial and temporal variations in growth rates along active normal fault systems: An example from The Lazio–Abruzzo Apennines, central Italy. *Journal of Structural Geology*, *26*(2), 339–376. https://doi.org/10.1016/S0191-8141(03)00103-2

Rosenbaum, G., Weinberg, R. F., & Regenauer-Lieb, K. (2008). The geodynamics of lithospheric extension. *Tectonophysics*, *458*(1), 1–8. https://doi.org/10.1016/j.tecto.2008.07.016

Royden, L., Patacca, E., & Scandone, P. (1987). Segmentation and configuration of subducted lithosphere in Italy: An important control on thrust-belt and foredeep-basin evolution. *Geology*, *15*(8), 714–717. https://doi.org/10.1130/0091-7613(1987)15<714:SACOSL>2.0.CO;2

Sage, L., Mosconi, A., Moretti, I., Riva, E., & Roure, F. (1991). Cross section balancing in the central Apennines: An application of LOCACE. *AAPG Bulletin*, *75*(4), 832–844. https://doi.org/10.1306/0C9B2867-1710-11D7-8645000102C1865D

Salvini, F. (2019). Daisy 3: The structural data integrated system analyzer version 5.57-22b [Software]. *University of Roma Tre*.

Salvini, F., & Vittori, E. (1982). Analisi strutturale della linea Olevano-Antrodoco-Posta (Ancona-Anzio Auct.): Metodologia di studio delle deformazioni fragili e presentazione del tratto meridionale. *Memorie della Societa Geologica Italiana*, *24*, 337–355.

San Jose, M., Caves Rugenstein, J. K., Cosentino, D., Faccenna, C., Fellin, M. G., Ghinassi, M., & Martini, I. (2020). Stable isotope evidence for rapid uplift of the central Apennines since the late Pliocene. *Earth and Planetary Science Letters*, *544*, 116376. https://doi.org/10.1016/j.epsl.2020.116376

Sawyer, D. S., Coffin, M. F., Reston, T. J., Stock, J. M., & Hopper, J. R. (2007). COBBOOM: The continental breakup and birth of oceans mission. *Scientific Drilling*, *5*, 13–25. https://doi.org/10.2204/iodp.sd.5.02.2007

Serpelloni, E., Faccenna, C., Spada, G., Dong, D., & Williams, S. D. P. (2013). Vertical GPS ground motion rates in the Euro-Mediterranean region: New evidence of velocity gradients at different spatial scales along the Nubia-Eurasia plate boundary. *Journal of Geophysical Research: Solid Earth*, *118*(11), 6003–6024. https://doi.org/10.1002/2013JB010102

Sharp, Z. (2017). Principles of stable isotope geochemistry. https://doi.org/10.25844/h9q1-0p82

Shen, C.-C., Wu, C.-C., Cheng, H., Lawrence Edwards, R., Hsieh, Y.-T., Gallet, S., et al. (2012). High-precision and high-resolution carbonate ^{230}Th dating by MC-ICP-MS with SEM protocols. *Geochimica et Cosmochimica Acta*, *99*, 71–86. https://doi.org/10.1016/j.gca.2012.09.018

Sheppard, S. M. F., & Schwarcz, H. P. (1970). Fractionation of carbon and oxygen isotopes and magnesium between coexisting metamorphic calcite and dolomite. *Contributions to Mineralogy and Petrology*, *26*, 161–198. https://doi.org/10.1007/BF00373200

Smeraglia, L., Berra, F., Billi, A., Boschi, C., Carminati, E., & Doglioni, C. (2016). Origin and role of fluids involved in the seismic cycle of extensional faults in carbonate rocks. *Earth and Planetary Science Letters*, *450*, 292–305. https://doi.org/10.1016/j.epsl.2016.06.042

Soliva, R., Benedicto, A., Schultz, R. A., Maerten, L., & Micarelli, L. (2008). Displacement and interaction of normal fault segments branched at depth: Implications for fault growth and potential earthquake rupture size. *Journal of Structural Geology*, *30*(10), 1288–1299. https://doi.org/10.1016/j.jsg.2008.07.005

Spadi, M., Gliozzi, E., Cosentino, D., & Nocentini, M. (2016). Late Piacenzian–Gelasian freshwater ostracods (Crustacea) from the L'Aquila Basin (central Apennines, Italy). *Journal of Systematic Palaeontology*, *14*(7), 617–642. https://doi.org/10.1080/14772019.2015.1079561

Spadi, M., Gliozzi, E., & Medici, M. C. (2018). A Plio–Pleistocene Caspiocypris species flock (Candoninae, Ostracoda) from the Palaeolake Tiberino (Umbria, central Italy). *Journal of Systematic Palaeontology*, *16*(5), 417–434. https://doi.org/10.1080/14772019.2017.1310143

Spadi, M., Gliozzi, E., & Medici, M. C. (2019). Piacenzian–Gelasian non-marine ostracods from the Dunarobba Fossil Forest (Tiberino Basin, Umbria, central Italy). *Papers in Palaeontology*, *5*(3), 391–413. https://doi.org/10.1002/spp2.1240

Storti, F., Aldega, L., Balsamo, F., Corrado, S., Del Monaco, F., Di Paolo, L., et al. (2013). Evidence for strong middle Pleistocene earthquakes in the epicentral area of the 6 April 2009 L'Aquila seismic event from sediment paleofluidization and overconsolidation. *Journal of Geophysical Research: Solid Earth*, *118*(7), 3767–3784. https://doi.org/10.1002/jgrb.50254

Tallini, M., Cavuoto, G., Del Monaco, F., Di Fiore, V., Mancini, M., Caielli, G., et al. (2012). Seismic surveys integrated with geological data for in-depth investigation of Mt. Pettino active Fault area (Western L'Aquila Basin). *Italian Journal of Geosciences*, *131*(3), 389–402. https://doi.org/10.3301/IJG.2012.10

Tallini, M., Spadi, M., Cosentino, D., Nocentini, M., Cavuoto, G., & Di Fiore, V. (2019). High-resolution seismic reflection exploration for evaluating the seismic hazard in a Plio-Quaternary intermontane basin (L'Aquila downtown, central Italy). *Quaternary International*, *532*, 34–47. https://doi.org/10.1016/j.quaint.2019.09.016

Tavani, S., Smeraglia, L., Fabbi, S., Aldega, L., Sabbatino, M., Cardello, G. L., et al. (2023). Timing, thrusting mode, and negative inversion along the Circeo thrust, Apennines, Italy: How the accretion-to-extension transition operated during slab rollback. *Tectonics*, *42*(6), e2022TC007679. https://doi.org/10.1029/2022TC007679

Trudgill, B., & Cartwright, J. (1994). Relay-ramp forms and normal-fault linkages, Canyonlands National Park, Utah. *GSA Bulletin*, *106*(9), 1143–1157. https://doi.org/10.1130/0016-7606(1994)106<1143:RRFANF>2.3.CO;2

Van Wijk, J. W., & Blackman, D. K. (2005). Dynamics of continental rift propagation: The end-member modes. *Earth and Planetary Science Letters*, *229*(3), 247–258. https://doi.org/10.1016/j.epsl.2004.10.039

Vezzani, L., & Ghisetti, F. (1998). Carta geologica dell'Abruzzo.

Villani, F., Improta, L., Pucci, S., Civico, R., Bruno, P. P. G., & Pantosti, D. (2016). Investigating the architecture of the Paganica Fault (2009 Mw 6.1 earthquake, central Italy) by integrating high-resolution multiscale refraction tomography and detailed geological mapping. *Geophysical Journal International*, *208*(1), 403–423. https://doi.org/10.1093/gji/ggw407

Vittori, E., Di Manna, P., Blumetti, A. M., Comerci, V., Guerrieri, L., Esposito, E., et al. (2011). Surface Faulting of the 6 April 2009 Mw 6.3 L'Aquila Earthquake in central Italy. *Bulletin of the Seismological Society of America*, *101*(4), 1507–1530. https://doi.org/10.1785/0120100140

Walsh, J. J., Bailey, W. R., Childs, C., Nicol, A., & Bonson, C. G. (2003). Formation of segmented normal faults: A 3-D perspective. *Journal of Structural Geology*, *25*(8), 1251–1262. https://doi.org/10.1016/S0191-8141(02)00161-X

Walsh, J. J., & Watterson, J. (1991). Geometric and kinematic coherence and scale effects in normal fault systems. *Geological Society, London, Special Publications*, *56*(1), 193–203. https://doi.org/10.1144/GSL.SP.1991.056.01.13

Zwaan, F., Schreurs, G., Naliboff, J., & Buiter, S. J. H. (2016). Insights into the effects of oblique extension on continental rift interaction from 3D analogue and numerical models. *Tectonophysics*, *693*, 239–260. https://doi.org/10.1016/j.tecto.2016.02.036

References From the Supporting Information

Bernasconi, S. M., Daëron, M., Bergmann, K. D., Bonifacie, M., Meckler, A. N., Affek, H. P., et al. (2021). InterCarb: A community effort to improve interlaboratory standardization of the carbonate clumped isotope thermometer using carbonate standards. *Geochemistry, Geophysics, Geosystems*, *22*(5), e2020GC009588. https://doi.org/10.1029/2020GC009588

Brand, W. A., Assonov, S. S., & Coplen, T. B. (2010). Correction for the ^{17}O interference in $\delta(^{13}C)$ measurements when analyzing CO_2 with stable isotope mass spectrometry (IUPAC Technical Report). *Pure and Applied Chemistry*, *82*(8), 1719–1733. https://doi.org/10.1351/PAC-REP-09-01-05

Daëron, M. (2021). Full propagation of analytical uncertainties in Δ_{47} measurements. *Geochemistry, Geophysics, Geosystems*, *22*(5), e2020GC009592. https://doi.org/10.1029/2020GC009592

Daëron, M., Blamart, D., Peral, M., & Affek, H. P. (2016). Absolute isotopic abundance ratios and the accuracy of Δ_{47} measurements. *Chemical Geology*, *442*, 83–96. https://doi.org/10.1016/j.chemgeo.2016.08.014

De Vleeschouwer, D., Peral, M., Marchegiano, M., Füllberg, A., Meinicke, N., Pälike, H., et al. (2022). Plio-Pleistocene Perth Basin water temperatures and Leeuwin Current dynamics (Indian Ocean) derived from oxygen and clumped-isotope paleothermometry. *Climate of the Past*, *18*(5), 1231–1253. https://doi.org/10.5194/cp-18-1231-2022

Heath, M., Phillips, D., & Matchan, E. L. (2018). An evidence-based approach to accurate interpretation of $^{40}Ar/^{39}Ar$ ages from basaltic rocks. *Earth and Planetary Science Letters*, *498*, 65–76. https://doi.org/10.1016/j.epsl.2018.06.024

Lee, J.-Y., Marti, K., Severinghaus, J. P., Kawamura, K., Yoo, H.-S., Lee, J. B., & Kim, J. S. (2006). A redetermination of the isotopic abundances of atmospheric Ar. *Geochimica et Cosmochimica Acta*, *70*(17), 4507–4512. https://doi.org/10.1016/j.gca.2006.06.1563

Ludwig, K. R. (2003). *User's manual for isoplot 3.00: A geochronological toolkit for Microsoft Excel (Issue 4)*. Kenneth R.

Matchan, E. L., & Phillips, D. (2014). High precision multi-collector $^{40}Ar/^{39}Ar$ dating of young basalts: Mount Rouse volcano (SE Australia) revisited. *Quaternary Geochronology*, *22*, 57–64. https://doi.org/10.1016/j.quageo.2014.02.005

McDougall, I., & Harrison, T. M. (1999). *Geochronology and thermochronology by the $^{40}Ar/^{39}Ar$ method*. Oxford University Press.

Moore, D. M., & Reynolds, R. C.Jr. (1997). *X-Ray diffraction and the identification and analysis of clay minerals* (p. 378). Oxford University Press.

Petersen, S. V., Defliese, W. F., Saenger, C., Daëron, M., Huntington, K. W., John, C. M., et al. (2019). Effects of improved ^{17}O correction on interlaboratory agreement in clumped isotope calibrations, estimates of mineral-specific offsets, and temperature dependence of acid digestion fractionation. *Geochemistry, Geophysics, Geosystems*, *20*(7), 3495–3519. https://doi.org/10.1029/2018GC008127

Phillips, D., & Matchan, E. L. (2013). Ultra-high precision $^{40}Ar/^{39}Ar$ ages for Fish Canyon Tuff and Alder Creek Rhyolite sanidine: New dating standards required? *Geochimica et Cosmochimica Acta*, *121*, 229–239. https://doi.org/10.1016/j.gca.2013.07.003

Shen, C.-C., Cheng, H., Edwards, R. L., Moran, S. B., Edmonds, H. N., Hoff, J. A., & Thomas, R. B. (2003). Measurement of attogram quantities of ^{231}Pa in dissolved and particulate fractions of seawater by isotope dilution thermal ionization mass spectroscopy. *Analytical Chemistry*, *75*(5), 1075–1079. https://doi.org/10.1021/ac026247r

Steiger, R. H., & Jäger, E. (1977). Subcommission on geochronology: Convention on the use of decay constants in geo- and cosmochronology. *Earth and Planetary Science Letters*, *36*(3), 359–362. https://doi.org/10.1016/0012-821X(77)90060-7